



HHS Public Access

Author manuscript

Nat Biotechnol. Author manuscript; available in PMC 2022 June 09.

Published in final edited form as:

Nat Biotechnol. 2022 May ; 40(5): 731–740. doi:10.1038/s41587-021-01133-w.

Programmable deletion, replacement, integration, and inversion of large DNA sequences with twin prime editing

Andrew V. Anzalone^{1,2,3,*}, Xin D. Gao^{1,2,3,*}, Christopher J. Podracky^{1,2,3,*}, Andrew T. Nelson^{1,2,3}, Luke W. Koblan^{1,2,3}, Aditya Raguram^{1,2,3}, Jonathan M. Levy^{1,2,3}, Jaron A. M. Mercer^{1,2,3}, David R. Liu^{1,2,3,†}

¹Merkin Institute of Transformative Technologies in Healthcare, Broad Institute of Harvard and MIT, Cambridge, Massachusetts, USA

²Department of Chemistry and Chemical Biology, Harvard University, Cambridge, Massachusetts, USA

³Howard Hughes Medical Institute, Harvard University, Cambridge, Massachusetts, USA

Abstract

The targeted deletion, replacement, integration, or inversion of genomic sequences could be used to study or treat human genetic diseases, but existing methods typically require double-strand DNA breaks (DSBs) that lead to undesired consequences including uncontrolled indel mixtures and chromosomal abnormalities. Here, we describe twin prime editing (twinPE), a DSB-independent method that uses a prime editor (PE) protein and two prime editing guide RNAs (pegRNAs) for the programmable replacement or excision of DNA sequences at endogenous human genomic sites. The two pegRNAs template the synthesis of complementary DNA flaps on opposing strands of genomic DNA, which replace the endogenous DNA sequence between the PE-induced nick sites. When combined with a site-specific serine recombinase, twinPE enabled targeted integration of gene-sized DNA plasmids (>5,000 bp) and targeted sequence inversions of 40 kb in human cells. TwinPE expands the capabilities of precision gene editing and may synergize with other tools for the correction or complementation of large or complex human pathogenic alleles.

Disease-associated human genetic variants range from single-base pair substitutions to mega base duplications, deletions and rearrangements¹⁻³. Gene editing approaches that can install, correct, or complement these pathogenic variants in human cells have the potential to advance our understanding of genetic disease and could also enable new therapeutics^{4,5}.

Users may view, print, copy, and download text and data-mine the content in such documents, for the purposes of academic research, subject always to the full Conditions of use: <https://www.springernature.com/gp/open-research/policies/accepted-manuscript-terms>

†Correspondence should be addressed to David R. Liu: drliu@fas.harvard.edu.

*These authors contributed equally

Author contributions

A.V.A., X.D.G., C.J.P., A.T.N., and J.M.L. designed experiments. A.V.A., X.D.G., C.J.P., A.T.N., L.W.K., A.R., and J.A.M.M. performed experiments and analyzed data. A.V.A., X.D.G., C.J.P. and D.R.L. wrote the manuscript. D.R.L. supervised the research.

Declaration of Interests

D.R.L. is a consultant and equity holder of Beam Therapeutics, Prime Medicine, Pairwise Plants, and Chroma Medicine, companies that use genome editing or genome engineering technologies. A.V.A., C.J.P., and J.M.L. are currently employees at Prime Medicine. A.V.A., X.D.G., C.J.P., and D.R.L. have filed patent applications on twinPE and prime editing through the Broad Institute.

Several mammalian cell gene editing approaches based on CRISPR-Cas systems have been developed over the past decade⁶, including nucleases⁷⁻⁹, base editors^{10,11}, and prime editors¹², each with the potential to address a subset of known pathogenic sequence changes.

CRISPR-Cas nucleases such as Cas9 can be used to disrupt genes by creating double-strand DNA breaks (DSBs) that lead to uncontrolled mixtures of indels. Additionally, paired Cas9 nuclease strategies can mediate targeted deletion of genomic DNA sequences ranging from ~50 to >100,000 base pairs in length¹³. By providing a linear donor DNA sequence, targeted insertion of new DNA sequences can be performed at single cut sites or between paired cut sites through end-joining or homology-directed repair (HDR) processes^{14,15}. Though versatile, single-nuclease and paired-nuclease editing approaches have substantial drawbacks. DNA donor knock-in is accompanied by efficient indel byproducts¹⁶, as HDR is generally inefficient compared to end-joining processes in most cell types^{17,18}. The use of paired nucleases for targeted deletion generates multiple byproducts^{13,19}, and the precise location of the deletions is restricted by PAM availability. Moreover, DSBs at on-target or off-target sites can promote large deletions²⁰⁻²², chromosomal abnormalities^{23,24}, and chromothripsis²⁵. The tendency of DSBs to generate complex mixtures of undesired byproducts and chromosomal changes²⁶⁻²⁸ poses considerable challenges when applying nuclease-based editing for the manipulation of larger DNA sequences, especially in therapeutic settings.

Base editors can precisely install single nucleotide mutations without requiring DSBs^{6,10,11}. Prime editors can precisely install any of the twelve possible base substitutions as well as small insertions and deletions without requiring DSBs¹². These DSB-free editing technologies cannot currently be used to directly install edits that alter thousands of base pairs. Prime editing has been shown to be capable of making precise insertions of up to ~40 bp and deletions of up to ~80 bp in human cells with high ratios of desired edits to byproducts¹². While prime editing offers the flexibility to replace one DNA sequence with another, PE2 and PE3 systems have not yet been able to mediate insertions or deletions the size of typical exons or gene coding sequences. These large DNA changes would presumably require long pegRNA reverse transcription templates and long-range DNA polymerization, eroding efficiency. In contrast, site-specific recombinases (SSRs) can excise, invert, and integrate large DNA sequences in mammalian cells²⁹. The longstanding challenge of reprogramming SSRs³⁰⁻³², however, has limited their use for precision gene editing applications.

Here, we report the development of twin prime editing (twinPE), which enables the deletion, substitution, or insertion of larger DNA sequences at targeted endogenous genomic sites with high efficiencies in human cells. We applied twinPE to efficiently insert recombinase recognition sites at different genomic loci in a programmable manner, allowing for targeted integration and inversion of gene-sized DNA segments.

Results

Twin prime editing strategy

Prime editing uses a prime editor protein containing a catalytically impaired Cas9 nickase and a wild-type (PE1) or engineered (PE2) reverse transcriptase (RT) enzyme, and a prime editing guide RNA (pegRNA) that both specifies the target genomic site and encodes the desired edit¹². Upon target site recognition, PE•pegRNA complexes nick the PAM-containing DNA strand and reverse transcribe the pegRNA's RT template into genomic DNA using the nicked strand as a primer. Following reverse transcription, the newly synthesized 3' flap containing the edited sequence invades the adjacent DNA to replace the redundant 5' flap sequence. The opposing nonedited strand is then repaired using the edited DNA strand as a template. This proposed prime editing pathway presents at least two opportunities for cellular DNA repair to reject the desired edit and revert the DNA sequence to its original form: during 3' flap annealing and ligation, and during heteroduplex resolution.

We hypothesized that bypassing these steps in DNA repair might allow prime editing to occur with increased efficiency and enable new classes of targeted gene edits in mammalian cells. We envisioned a twin prime editing (twinPE) strategy that uses a pair of pegRNAs, each targeting a different DNA strand, that each template the synthesis of a 3' flap that is complementary to the 3' flap templated by the other pegRNA (Fig. 1a). We hypothesized that if the newly synthesized DNA strands were highly dissimilar to the endogenous target site, the complementary 3' flaps would preferentially hybridize with each other to create an intermediate containing annealed 3' overhangs of new DNA sequence and annealed 5' overhangs of original DNA sequence (Fig. 1a). As both edited strands are synthesized by prime editor complexes, there is no requirement for strand invasion of the target site, or for the edit to be copied to the complementary DNA strand. Excision of the original DNA sequence (annealed 5' overhangs) and ligation of the pair of nicks would result in the replacement of the endogenous sequence with the paired 3' flap sequences (Fig. 1a). Due to the flexibility in template design, the edit could in principle insert a new DNA sequence, or delete or replace the original DNA sequence.

TwinPE-mediated large sequence replacement and deletion

To test the twinPE strategy, we initially targeted the HEK293T site 3 locus (hereafter referred to as *HEK3*) in HEK293T cells to replace 90 bp of endogenous sequence with a 38-bp Bxb1 integrase *attB* substrate sequence³³ (Fig. 1b). For each protospacer, three pegRNAs were designed with RT templates that contained 30, 34, or 38 nt of the 38-bp *attB* sequence (Fig. 1c). Pairwise combinations of these pegRNAs are predicted to generate 3' flaps with overlapping complementarity ranging from 22 to 38 bp (Fig. 1c). When both pegRNAs were transfected into HEK293T cells along with PE2, we observed highly efficient *attB* site insertion, with some combinations of pegRNAs yielding >80% conversion to the desired product (Fig. 1c). A similar strategy for the replacement of the 90-bp endogenous sequence with the 50-bp Bxb1 *attP* attachment sequence achieved editing efficiencies up to 58% (Fig. 1c). Notably, it was not necessary for either pegRNA to encode the full insertion sequence, since partially overlapping complementary flaps enabled full-length *attB* or *attP* sequence

incorporation, though 3' flaps with greater overlap led to slightly higher editing efficiencies and fewer indels (Fig. 1c).

Independent of our efforts, Shendure and co-workers³⁴ and Gao and co-workers³⁵ reported elegant dual-pegRNA prime editing systems that can be used to perform precise large deletions in human cells or improve base substitution and small insertion or deletion edits in plant cells, respectively. For each of these strategies, the templated 3' flap sequence is homologous to the target site DNA sequence to facilitate DNA repair for incorporation of the edit (Fig. 2a). In contrast, twinPE was designed to bypass the need for any homologous DNA sequence in the pegRNA RT template, offering more template sequence flexibility and the potential to make larger insertions with shorter RT templates. To test if twinPE could support the insertion of DNA sequences larger than the 44-bp insertions previously demonstrated¹² using PE2 or PE3, we compared the ability of twinPE and PE3 to generate a 108-bp *FKBP12* cDNA fragment insertion. Targeting the *HEK3* locus with PE3 in HEK293T cells, we achieved moderate editing efficiencies for the shorter 12-bp and 36-bp insertions (32% and 17%, respectively), but inefficient 108-bp insertion (0.80%) (Fig. 2b). In contrast, twinPE enabled 16% insertion efficiency for the 108-bp fragment with concomitant deletion of 90 bp of *HEK3* sequence, a 20-fold improvement. TwinPE was 2- to 4-fold more efficient than PE3 for inserting the 108-bp *FKBP12* cDNA fragment at *CCR5*, and inserted 113-bp and 103-bp sequences containing pairs of Bxb1 recombinase sites (*attB*-27 bp spacer-*attP* or *attB*-27 bp spacer-*attB*) at this locus with ~10% efficiency (Extended Data Fig. 1). Collectively, these results demonstrate the ability of twinPE to mediate larger insertions than have been previously demonstrated with PE2 and PE3 systems.

One potential application of the twinPE strategy is the replacement of mutated exonic coding sequence with DNA that encodes wild-type sequence. Such an approach has the potential to correct any combination of mutations between twinPE-induced nick sites and raises the possibility of using a single pegRNA set to correct multiple pathogenic mutations within a stretch of DNA. To test this approach, we targeted *PAH*, which encodes phenylalanine hydroxylase. Mutations within *PAH* cause the genetic metabolic disorder phenylketonuria (PKU)³⁶. We tested the ability of twinPE to recode portions of *PAH* exon 4 and exon 7, which commonly harbor mutations in PKU patients, in HEK293T cells. By testing different flap overlap lengths using engineered pegRNAs (epegRNAs) containing a 3' evoPreQ1 motif³⁷, we achieved the desired sequence recoding with efficiencies of 23% for a 46-bp recoding in exon 7, 27% for 64-bp recoding in exon 7, and 9.4% for a 64-bp recoding in exon 4 (Fig. 2c and Extended Data Fig. 2). Additional exons in *PAH* could also be recoded, albeit with lower efficiency (Extended Data Fig. 2). These results demonstrate that twinPE can replace stretches of dozens of nucleotides in human cells with a single pair of pegRNAs.

In addition to insertion and replacement of DNA sequences, twinPE may also mediate precise deletions more effectively and with greater flexibility than previously described methods. We compared three strategies using paired pegRNAs: a “single-anchor” (SA) twinPE strategy, which fixes the deletion junction at one of the two nick sites; a “hybrid-anchor” (HA) twinPE strategy, which allows flexible deletion junctions between the nick sites; and the PrimeDel (PD) strategy recently reported by Shendure and coworkers³⁴, which

generates deletions between the nick sites with the option of inserting additional DNA sequence (Fig. 2d). These strategies differ in the relationship of the sequences of the two flaps and the positioning of the deletion with respect to the nick sites (Fig. 2d).

Targeting the *HEK3* site in HEK293T cells using the single-anchor strategy, 13-nt complementary flaps were used to delete 77 bp adjacent to one of the pegRNA-induced nick sites with 15% efficiency and 2.1% indels (Fig. 2e, SA- 77), and 34-nt complementary flaps were used to precisely excise 56 bp of sequence with 19% efficiency and 4.2% indels (Fig. 2e, SA- 56). Using the hybrid-anchor strategy, we deleted 64 bp between the pegRNA-induced nick sites such that the product retains 13 bp of sequence 3' of each nick with 12% efficiency and 5.5% indels (Fig. 2e, HA- 64). Finally, we tested the PrimeDel strategy for the deletion of 90 bp between the pegRNA-induced nick sites, which occurred with 40% efficiency and 1.6% indels (Fig. 2e, PD- 90). The higher efficiency of the PrimeDel strategy may arise from its ability to disrupt the PAM sequences on both strands, which likely increases deletion efficiency by limiting target re-engagement that can lead to indels or re-nicking of the prime-edited strand. Editing efficiencies were improved for all three approaches by 1.5-fold to 2.5-fold upon the addition of the evoPreQ1 motif the 3' end of the resulting epegRNAs³⁷ (Fig. 2e). Together, these data show that twinPE offers a strategy for performing targeted deletions with high flexibility and high product purity that does not rely on the availability of nuclease cut sites.

We applied twinPE-mediated deletions to target *DMD*. Pathogenic *DMD* alleles, which cause Duchenne muscular dystrophy, commonly contain large deletions in exonic regions that result in frameshifted transcripts³⁸. Because production of nearly full-length dystrophin protein without replacement of the deleted exons can partially rescue protein function, deletion of another exon to restore the reading frame has been pursued as a therapeutic strategy³⁹. We examined three twinPE deletion strategies along with a previously reported Cas9 nuclease deletion strategy for excising exon 51 in *DMD*³⁹. Using single-anchor twinPE deletion approaches, we observed 28% average efficiency for deletion of a 780-bp sequence containing *DMD* exon 51 (Fig. 2f). Exon 51 of *DMD* could also be excised using alternative spacer pairs that generate a 627-bp deletion with the PrimeDel strategy (30% average efficiency) or by using twinPE to replace a 589-bp sequence with a 38-bp Bxb1 *attB* sequence (40% average efficiency) (Fig. 2f). While the paired sgRNA Cas9 nuclease strategy for deleting 818 bp achieved higher efficiency (averaging 50% precise deletion) compared to twinPE, the deletion was also accompanied by much higher indel levels of 45% (33% desired deletion with additional indels, plus 12% indels without the desired deletion) compared to twinPE, which averaged 5.1% total indels (Fig. 2f). These experiments show that twinPE and PrimeDel can generate large deletions at therapeutically relevant loci in human cells with far fewer indel byproducts compared to paired Cas9 nuclease strategies.

To examine potential off-target editing by twinPE, we amplified and sequenced four previously characterized off-target loci for one of the *HEK3* spacer sequences following treatment by eight different sets of twinPE reagents targeting *HEK3* (SA- 77, SA- 56, HA- 64, and PD- 90 with standard pegRNAs and epegRNAs). For each of the eight twinPE treatments, no detectable off-target edits or indels were detected at any of the four off-target sites beyond background levels in untreated control samples (Supplementary Table 5). The

requirement for multiple hybridization events (pegRNA spacer to genome, pegRNA PBS to nicked genomic DNA primer, and synthesized 3' DNA flap to either the genome in standard PE or the second 3' DNA flap in twinPE) may explain the low off-target editing of prime editing compared to Cas9 nuclease as observed by our group and others^{12,40,41}.

Site-specific DNA integration at safe harbor loci with twinPE and Bxb1 integrase

Although twinPE can mediate large insertions more efficiently than PE3, the upper limit of sequence insertion we observed with twinPE was ~100 bp. To integrate larger DNA cargo, we combined twinPE with a site-specific integrase (Fig. 3a). Researchers have previously used Bxb1 integrase to integrate large DNA segments into pre-installed *attB* and *attP* sites in mammalian cells⁴². To identify sites for cargo integration, we first tested twinPE-mediated insertion of Bxb1 *attB* and *attP* sequences at established safe harbor loci in HEK293T cells. We screened 15 spacer pairs with three PBS variants per pegRNA (135 pegRNA pairs total) for insertion of the 38-bp Bxb1 *attB* sequence at *CCR5* (Extended Data Fig. 3). Optimal pegRNAs for six of these spacer pairs achieved >50% editing efficiency with 3.9–5.4% indel byproducts (Fig. 3b). Likewise, 32 spacer pairs (288 pegRNA pairs total) targeting *AAVS1* were screened for insertion of the 50-bp Bxb1 *attP* sequence (Extended Data Fig. 4). Optimal pegRNAs for 17 of these spacer pairs achieved >50% efficiency with a median of 6.6% indels (Fig. 3c). Notably, twinPE outperformed PE3 for insertion of *attB* at *CCR5* in HEK293T cells (Extended Data Fig. 5). These results demonstrate that twinPE can be used to insert recombinase target sites at safe harbor loci in human cells with high efficiency.

Next, we examined if twinPE-inserted Bxb1 attachment sequences could serve as substrates for the integration of DNA plasmids. We used twinPE to generate a clonal HEK293T cell line with a homozygous *attB* insertion at *CCR5*. Transfection of this cell-line with a plasmid expressing codon-optimized Bxb1 and a 5.6-kb *attP*-containing DNA donor plasmid resulted in 12–17% knock-in of the donor plasmid at *CCR5*, as measured by ddPCR quantification of an amplicon spanning the donor-genome junction and comparison to a reference amplicon in *ACTB* (Extended Data Fig. 6). This knock-in efficiency is consistent with previously reported Bxb1-mediated plasmid integration efficiencies in mammalian cells⁴³.

We next explored whether the components for twinPE-mediated attachment site insertion and Bxb1-mediated recombination could achieve donor integration in a single transfection step. Our initial transfection of HEK293T cells with plasmids encoding PE2, both pegRNAs, Bxb1, and a 5.6-kb donor plasmid resulted in 1.4–6.8% knock-in efficiency as measured by ddPCR (Fig. 3d). The anticipated junction sequences containing *attL* and *attR* recombination products were confirmed by amplicon sequencing, with very high product purities (84.8–99.9%, 99.3% median) (Extended Data Fig. 6).

To optimize single-transfection targeted donor integration, we investigated the effects of genomic attachment site (*attB* vs. *attP*), attachment site central dinucleotide (wild-type GT vs. mutant GA)⁴³, and the length of 3' flap overlapping complementarity on knock-in efficiency. We found that knock-in was more efficient when twinPE was used to insert *attB* rather than *attP*, especially when pegRNAs encoded full-length *attB* or *attP* (3.3% vs. 0.5% targeted integration, Fig. 3e). We also observed that the wild-type GT central dinucleotide supported higher knock-in efficiencies than GA (Fig. 3e). Notably, attachment

sites with different central dinucleotides are orthogonal to one another⁴³, which allowed multiplexed knock-in of an *attB*-GT donor at an *attP*-GT site in *AAVS1* and GA donors at GA attachment sites in *CCR5* (Extended Data Fig. 6). Reducing 3' flap overlap improved single-transfection targeted plasmid integration efficiency from 3.3±0.2% with 38 base pairs of overlap to 5.5±0.6% with 20 base pairs of overlap when inserting *attB*, and from 0.55±0.1% with 50 base pairs of overlap to 4.1±0.8% with 30 base pairs of overlap when inserting *attP* (Fig. 3e). Similar twinPE efficiencies were observed for *attB* insertion with long (38-bp) or short (20-bp) flap overlaps. Recombination between *attP*-containing donor DNA and pegRNA expression plasmid was observed when the pegRNAs had 38-bp of overlap but was not detected when with pegRNA plasmids encoding 20-bp flap of flap overlap (Extended Data Fig. 6). The enhanced knock-in efficiency with partially overlapping flaps may arise from reducing or eliminating unproductive recombination between donor and pegRNA expression plasmid DNA.

We next applied plasmid integration via twinPE and Bxb1 recombination at *ALB*, which has been investigated clinically for therapeutic transgene expression in hepatocytes^{44,45}. Given high albumin expression in the liver, therapeutic transgene integration at *ALB* in a small percentage of hepatocytes could produce clinically relevant protein levels for many loss-of-function diseases⁴⁴. For example, increasing circulating Factor IX levels to just 1% of normal is therapeutic for the treatment of hemophilia⁴⁵. We devised a strategy in which twinPE targets intron 1 of *ALB* and Bxb1 integrates a donor bearing a splice acceptor followed by the cDNA for a protein of interest. Following integration, splicing of the secretion signal in *ALB* exon 1 to the therapeutic transgene enables its expression and secretion.

We screened pegRNA pairs for the twinPE-mediated insertion of *attB* within intron 1 of *ALB* (Fig. 3f) and identified a spacer combination that achieved 43% correct insertion of the *attB* sequence. Single-transfection integration of a mock donor plasmid (a promoter-less copy of EGFP and PuroR-T2A-BFP under control of the EF1 α promoter; 5.6-kb total) proceeded with 1.3% efficiency in HEK293T cells (Fig. 3g). In Huh7 cells, we observed 34% correct insertion of the *attB* sequence (Fig. 3f) and achieved single-transfection targeted knock-in efficiency of 2.6%. Transfection of Huh7 cells with plasmids encoding Bxb1, PE2, pegRNAs for *attB* insertion in *ALB* intron 1, and an *attP*-containing donor bearing a splice acceptor and the cDNA for human factor IX (hFIX) exons 2-8 led to detectable levels of hFIX in conditioned media (Extended Data Fig. 7). No hFIX was detected when the pegRNAs targeted *CCR5* instead of *ALB*. Collectively, these results establish a method for the integration of gene-sized DNA sequences at targeted genomic loci in previously unmodified human cells without double strand breaks or HDR.

To assess the possibility of undesired Bxb1-mediated donor integration or sequence modifications at off-target sites in the human genome, we selected five Bxb1 pseudo-sites for further characterization. Pseudo-sites were nominated based on the presence of a minimal Bxb1 recognition motif (ACNACNGNNNNNCNGTNGT) identified by recombinase specificity profiling⁴⁶, and a GT central dinucleotide matching the donor plasmid used in our experiments⁴³. Amplicon sequencing of all five nominated pseudo-sites in seven different samples treated with donor plasmid, twinPE reagents targeting *CCR5* or

AAVSI, and Bxb1 recombinase showed undetectable (<0.1%) or near-background levels of indels compared to untreated controls (Extended Data Fig. 7). To capture donor plasmid integration events at the nominated pseudo-sites, we attempted to amplify the expected integration junctions from treated genomic DNA samples. We observed no PCR products corresponding to off-target donor integration at any pseudo-site in any sample, while amplicons corresponding to on-target donor integration were readily observed (Extended Data Fig. 7). These results demonstrate that twinPE+Bxb1 can mediate precise donor integration at the intended target site without generating detectable levels of undesired donor integration or sequence alteration at predicted Bxb1 pseudo-sites in the human genome.

TwinPE and recombinase-mediated large inversions

Large structural variants are found in many human pathogenic alleles¹⁻³. Given the high efficiency of recombinase attachment site insertions using twinPE, we reasoned that multiplexing the insertion of Bxb1 *attB* and *attP* could be used to correct complex genetic variants by deleting or inverting the intervening DNA sequence. We first tested whether twinPE and Bxb1 could revert an inverted H2B-EGFP coding sequence stably integrated into the HEK293T genome via lentiviral transduction (Extended Data Fig. 8). After transfection of the reporter cells with PE2, four pegRNAs, and Bxb1, we observed up to 19% GFP positive cells by flow cytometry, indicating successful inversion (Extended Data Fig. 8).

To test the twinPE-recombinase inversion approach at a therapeutically relevant locus, we performed a 40-kb inversion between *IDS* and its pseudogene *IDS2*. Inversions between these sites have been observed in ~13% of Hunter syndrome patients⁴⁷, and characterization of the breakpoints in pathogenic alleles revealed that the inversion often occurs within a recombination hotspot that is present in both *IDS* and *IDS2*⁴⁷. We targeted regions flanking these recombination hotspots for the insertion of *attB* and *attP* sequences, which allow unidirectional inversion by Bxb1 to correct the pathogenic allele when present in opposing orientations (Fig. 4a). After screening pegRNAs, we found pegRNAs that are capable of inserting *attB* or *attP* sites at the left and right targeted sites with 70% and 74% efficiency, respectively in HEK293T cells (Fig. 4b).

Next, we explored multiplexed twinPE insertion of *attB* and *attP* sites with Bxb1-mediated inversion of the 40-kb sequence in *IDS* and *IDS2*. We performed sequential DNA transfections with twinPE components followed by Bxb1. An initial set of pegRNAs (set 1) was tested that installs a reverse-oriented *attP* sequence in intron 3 of *IDS2* and a forward-oriented *attB* sequence in intron 7 of *IDS*. A second set of pegRNAs (set 2) was used to install a forward-oriented *attP* sequence in *IDS2* and a reverse-oriented *attB* sequence in *IDS*. We observed 52% or 55% *attP* insertion and 28% or 31% *attB* insertion for multiplexed editing with pegRNA set 1 and set 2, respectively (Fig. 4c). When edited cells were transfected with Bxb1 recombinase, we observed a significant decrease in the percentage of amplified alleles containing *attP* and *attB* sequences compared to mock transfection controls (p-value < 0.05), suggesting that the some pairs of sites had recombined (Fig. 4c). Amplicon sequencing of the anticipated inversion junctions revealed the presence of both *attL* and *attR* recombination products with product purity 80% at both junctions (Fig. 4d).

To circumvent unwanted recombination between pegRNA expression plasmids when combining twinPE and Bxb1-mediated inversion in a single step, we nucleofected HEK293T cells with PE2 mRNA, synthetic pegRNAs from set 1, and Bxb1 mRNA. Using amplicon sequencing, we captured the expected inverted allele junctions containing *attR* and *attL* sequences (Extended Data Fig. 9). To quantify inversion efficiency, we designed a reverse primer that binds to identical sequences in both the non-inverted and inverted alleles, allowing amplification of both alleles using the same primer pair (Extended Data Fig. 9). We observed 7.7–9.6% and 2.1–2.6% inversion efficiency for sequential and one-step methods, respectively (Fig. 4e). Collectively, these data suggest that combining twinPE with site-specific serine recombinases can be used to correct a common 39-kb inversion that causes Hunter syndrome and may eventually serve as a therapeutic strategy for correcting other large or complex pathogenic gene variants.

Discussion

We developed a twin prime editing approach that can be used to replace, insert, or delete DNA sequences at targeted locations in the genomes of human cells. TwinPE can efficiently replace endogenous genomic DNA sequences with exogenous sequences containing Bxb1 *attB* or *attP* sites at a variety of genomic loci in HeLa, U2OS, and K562 cells (Extended Data Fig. 10). An active RT is required for editing, as Cas9 nickase (H840A) and Cas9 nickase fused to an inactivated RT (K103L/R110S) both failed to generate the desired edits at all sites tested (Extended Data Fig. 10). We used twinPE to recode portions of exon sequences within *PAH*, which in principle could be used to correct multiple pathogenic variants using a pegRNA pair. Moreover, because twinPE does not require pegRNA RT templates to possess homology to the target site or encode the entire replacement sequence, twinPE pegRNAs can encode larger insertions for a given RT template length, including the insertion of a 108-bp sequence with 16% efficiency using twinPE, representing a 20-fold improvement over PE3. Although the design principles governing twinPE pegRNA performance are not yet fully understood (Supplementary Note 3), the use of epegRNAs³⁷ generally improved twinPE (Fig. 2c, 2e, Extended Data Fig 9). Empirical testing of epegRNA pairs is important to optimize twinPE efficiency.

We demonstrated precise and flexible twinPE deletion strategies that make use of the programmability of 3' flap sequences to fully specify deletion junctions, a limitation of nuclease-based deletion strategies. Using twinPE, we tested three deletion strategies, including the previously reported PrimeDel strategy³⁴. TwinPE achieved precise deletions of up to 780-nt in *DMD* including the deletion of exon 51 with up to 28% efficiency and only 5.1% indels. Although Cas9 nuclease-mediated deletion at this site achieved 50% perfect deletion efficiency, it generated 45% indels in the process. TwinPE may be especially useful for applications in which uncontrolled indel byproducts or other DSB consequences are problematic.

When combined with site-specific serine recombinases, twinPE can support the integration of large DNA cargo and the inversion of large DNA sequences. TwinPE and Bxb1 in a single transfection successfully inserted a 5.6-kb DNA donor plasmid into the genomes of human cells at *AAVS1*, *CCR5*, and *ALB* with 6.8%, 6.1%, and 2.6% efficiency, respectively. This

RNA-programmable method for targeted gene-sized insertions has several advantages over other methods that use zinc-finger recombinases³², DSBs^{14,15}, and HDR⁴⁸ (Supplemental Note 4). Given that twinPE insertion of *attB* and *attP* sequences can already exceed 80%, improving recombinase efficiency represents a promising strategy for enhancing targeted knock-in efficiencies.

We used multiplex twinPE insertion of *attP* and *attB* and Bxb1 to perform a 40 kb sequence inversion at *IDS* and *IDS2* that is associated with Hunter syndrome with 9.6% and 2.6% efficiency via sequential transfection and one-step RNA nucleofection, respectively (Fig. 4e). Although nuclease approaches have achieved targeted sequence inversions previously^{49,50}, DSB-induced repair pathways generate undesired products and can lead to *de-novo* structural variants, including deletion of the targeted DNA sequence²⁰⁻²² and chromosomal abnormalities^{23,24}. TwinPE and Bxb1 achieves comparable efficiency while circumventing the uncontrolled nature of DSB repair.

In summary, twinPE expands the capabilities of prime editing to include targeted deletion, replacement, and, when combined with site-specific recombinases, gene-sized integration and inversion without requiring double-strand breaks. These new capabilities may enable strategies to study and treat genetic diseases arising from loss-of-function or complex structural mutations.

Methods

General methods.

DNA amplification was conducted by PCR using Phusion U Green Multiplex PCR Master Mix (ThermoFisher Scientific) or Q5 Hot Start High-Fidelity 2x Master Mix (New England BioLabs) unless otherwise noted. DNA oligonucleotides were obtained from Integrated DNA Technologies. Plasmids expressing sgRNAs were constructed by ligation of annealed oligonucleotides into *BsmBI*-digested acceptor vector as previously described¹. Plasmids expressing pegRNAs were constructed by Gibson assembly or Golden Gate assembly as previously described¹. Sequences of sgRNA and pegRNA constructs used in this work are listed in Supplementary Table 1. All vectors for mammalian cell experiments were purified using Plasmid Plus Midiprep kits (Qiagen), PureYield plasmid miniprep kits (Promega), or QIAprep Spin Miniprep kits. Synthetic pegRNAs were ordered from IDT without HPLC purification.

General mammalian cell culture conditions.

HEK293T (ATCC CRL-3216), U2OS (ATTC HTB-96), K562 (ATCC CCL-243), and HeLa (ATCC CCL-2) cells were purchased from ATCC and cultured and passaged in Dulbecco's Modified Eagle's Medium (DMEM) plus GlutaMAX (ThermoFisher Scientific), McCoy's 5A Medium (Gibco), RPMI Medium 1640 plus GlutaMAX (Gibco), or Eagle's Minimal Essential Medium (EMEM, ATCC), respectively, each supplemented with 10% (v/v) fetal bovine serum (Gibco, qualified) and 1x Penicillin+Streptomycin (Corning). Huh7 cells (a gift from Erik Sontheimer's group. Originated from ATCC) were cultured and passaged in Dulbecco's Modified Eagle's Medium (DMEM) plus GlutaMAX (ThermoFisher

Scientific) supplemented with 10% (v/v) fetal bovine serum (Gibco, qualified) and 1x Penicillin+Streptomycin (Corning). All cell types were incubated, maintained, and cultured at 37 °C with 5% CO₂. Cell lines were authenticated by their respective suppliers and tested negative for mycoplasma.

HEK293T, HeLa, and Huh7 tissue culture transfection protocol and genomic DNA preparation.

HEK293T cells were seeded on 48-well poly-D-lysine coated plates (Corning). 16-24 h post-seeding, cells were transfected at approximately 60% confluency with 1 µL of Lipofectamine 2000 (Thermo Fisher Scientific) according to the manufacturer's protocols and either: 750 ng of PE2 plasmid DNA, 125 ng of pegRNA 1 plasmid DNA, and 125 ng of pegRNA 2 plasmid DNA (for twinPE transfections); 750 ng of PE2 plasmid DNA, 250 ng of pegRNA plasmid DNA, and 83 ng of sgRNA plasmid DNA (for PE3 transfections); or, 750 ng of Cas9 plasmid DNA and 125 ng of sgRNA 1 plasmid DNA, and 125 ng of sgRNA 2 plasmid DNA (for paired Cas9 nuclease transfections). Unless otherwise stated, cells were cultured 3 days following transfection, after which the media was removed, the cells were washed with 1x PBS solution (Thermo Fisher Scientific), and genomic DNA was extracted by the addition of 150 µL of freshly prepared lysis buffer (10 mM Tris-HCl, pH 7.5; 0.05% SDS; 25 µg/mL Proteinase K (ThermoFisher Scientific)) directly into each well of the tissue culture plate. The genomic DNA mixture was incubated at 37 °C for 1-2 h, followed by an 80 °C enzyme inactivation step for 30 min. Primers used for mammalian cell genomic DNA amplification are listed in Supplementary Table 2. For HeLa cell transfections, cells were grown and seeded in 96-well plates (Falcon Catalog #353075). 16-24 h post-seeding, cells were transfected 0.75 µL of TransIT-HeLaMONSTER transfection reagent (Mirus) using 190 ng of PE2-P2A-Blast plasmid DNA, 31.5 ng of pegRNA 1 plasmid DNA, and 31.5 ng of pegRNA 2 plasmid DNA (for twinPE transfections). 24 h after transfection, cells were treated with blasticidin to a final concentration of 10 µg/mL. Genomic DNA isolation was performed as described above for HEK293T cells using 50 µL of lysis buffer. Huh7 cells were seeded at 150,000 cells per well in poly-D-lysine coated 24-well plates (Corning). 16-24 h post-seeding, cells were transfected with 2 µL of Lipofectamine 2000 (Thermo Fisher Scientific) according to the manufacturer's protocols and up to 800 ng of plasmid DNA (same ratios as in HEK293T transfections described above, scaled proportionally). Genomic DNA isolation was performed as described above for HEK293T transfections.

High-throughput DNA sequencing of genomic DNA samples.

Genomic sites of interest were amplified from genomic DNA samples and sequenced on an Illumina MiSeq as previously described with the following modifications². Briefly, amplification primers containing Illumina forward and reverse adapters (Supplementary Table 2) were used for a first round of PCR (PCR 1) amplifying the genomic region of interest. 25-µL PCR 1 reactions were performed with 0.5 µM of each forward and reverse primer, 1 µL of genomic DNA extract and 12.5 µL of Phusion U Green Multiplex PCR Master Mix. PCR reactions were carried out as follows: 98 °C for 2 min, then 30 cycles of [98 °C for 10 s, 61 °C for 20 s, and 72 °C for 30 s], followed by a final 72 °C extension for 2 min. Unique Illumina barcoding primer pairs were added to each sample in a secondary PCR reaction (PCR 2). Specifically, 25 µL of a given PCR 2 reaction

contained 0.5 μM of each unique forward and reverse Illumina barcoding primer pair, 1 μL of unpurified PCR 1 reaction mixture, and 12.5 μL of Phusion U Green Multiplex PCR 2x Master Mix. The barcoding PCR 2 reactions were carried out as follows: 98 $^{\circ}\text{C}$ for 2 min, then 12 cycles of [98 $^{\circ}\text{C}$ for 10 s, 61 $^{\circ}\text{C}$ for 20 s, and 72 $^{\circ}\text{C}$ for 30 s], followed by a final 72 $^{\circ}\text{C}$ extension for 2 min. PCR products were evaluated analytically by electrophoresis in a 1.5% agarose gel. PCR 2 products (pooled by common amplicons) were purified by electrophoresis with a 1.5% agarose gel using a QIAquick Gel Extraction Kit (Qiagen), eluting with 40 μL of water. DNA concentration was measured by fluorometric quantification (Qubit, ThermoFisher Scientific) or qPCR (KAPA Library Quantification Kit-Illumina, KAPA Biosystems) and sequenced on an Illumina MiSeq instrument using Illumina MiSeq control software (v. 3.1) according to the manufacturer's protocols.

Sequencing reads were demultiplexed using MiSeq Reporter (Illumina). Alignment of amplicon sequences to a reference sequence was performed using CRISPResso2³. For all prime editing yield quantification, prime editing efficiency was calculated as: % of [# of reads with the desired edit that do not contain indels] \div [# of total reads]. For quantification of editing, CRISPResso2 was run in HDR mode using the desired allele as the expected allele (e flag), and with "discard_indel_reads" on. Any sequence containing an indels with respect to the allele to which it aligns was counted separately and did not contribute to the correctly edited allele percentage. The percent editing was quantified as the number of non-discarded reads aligning to the anticipated edited allele (not containing indels) divided by the total number of sequencing reads (which includes those aligned to reference with or without indels and those aligned to the desired edit with or without indels). Indels were quantified as the total number of discarded reads (from either the original or edited allele alignments) divided by the total number of sequencing reads. Editing yield was then calculated as: [# of non-discarded HDR aligned reads] \div [total reads]. Indel yields were calculated as: [# of indel-containing discarded reads] \div [total reads].

Unique molecular identifiers (UMIs) were applied to quantify the deletion efficiency and assess PCR bias (see Supplementary Note 1 for discussion) in a three-step PCR protocol. Briefly, in the first step of linear amplification, 1 μL of genomic DNA extract was linearly amplified by 0.1 μM of only the forward primer containing a 15-nt or 16-nt UMI with Phusion U Green Multiplex PCR Master Mix in a 25- μL reaction (10 cycles of 98 $^{\circ}\text{C}$ for 1 min, 61 $^{\circ}\text{C}$ for 25 s, and 72 $^{\circ}\text{C}$ for 1 min). The PCR products were then purified by 1.6X AmPure beads (Beckman Coulter) and eluted in 20 μL of QIAGEN elution buffer. In the second step, 1 or 2 μL of purified linearly amplified PCR products were then amplified for 30 cycles with 0.5 μM of each forward and reverse primer with Phusion U Green Multiplex PCR mix in a 25- μL reaction as described above. In this case, the forward primer anneals to the P5 Illumina adaptor sequence located at the 5' of the UMI primer and upstream of the UMI sequence. For the *DMD* locus library preparation, the PCR products were purified by 1X AmPure beads and eluted in 25 μL of elution buffer. In the third step, the purified PCR products (1 μL) were amplified for 12 cycles as described above for adding unique Illumina barcodes and adaptors. To assess large deletions at the *DMD* locus, the top band (unedited large amplicon) and bottom band (edited amplicons with deletions) were excised separately from a 1.5% agarose gel and loaded on two separate MiSeq runs to avoid biased clustering of amplicons. For library preparation at other loci, 1 μL of PCR product was used directly

for the barcoding PCR step without 1X AmPure beads purification. For UMI-based PCR bias assessment described in Supplementary Note 1, the editing efficiency was calculated from the libraries prepared following the UMI protocols analyzed with UMI-deduplication or without UMI-deduplication.

Raw sequencing reads were UMI deduplicated using AmpUMI⁴. For paired-end reads, SeqKit⁵ was used to concatenate (merge without overlap) R1s with the reverse complement of R2s. The concatenated R1+R2s were UMI deduplicated using the UMI at the 5' end of R1. UMI-deduplicated R1s or concatenated R1+R2s were analyzed using CRISPResso2. For analyzing concatenated R1+R2s, an appropriate concatenated reference amplicon sequence was provided to minimize sequencing alignment artifacts due to the concatenation.

Nucleofection of U2OS and K562.

Nucleofection was performed in all experiments that used K562 and U2OS cells. 200,000 cells were used per nucleofection. Counted cells were pelleted and washed with PBS, then resuspended in nucleofection solution following the recommendation of Lonza SE Cell Line 4D-Nucleofector Kit. After nucleofection of the cells, the cells were allowed to incubate in the cuvette at room temperature for 10 minutes. After this time, the contents of the cuvette were transferred to a 48 well plate containing pre-warmed (37 °C) media. Genomic DNA was extracted and prepared for Illumina MiSeq preparation as described above.

Single-step twinPE and Bxb1-mediated DNA donor knock-in and inversions.

For single-step knock-in, HEK293T cells were transfected with 500 ng of PE2 plasmid DNA, 50 ng of each pegRNA plasmid DNA (two in total), 200 ng of codon-optimized Bxb1 plasmid DNA, and 200 ng of DNA donor using Lipofectamine 2000 as described above. For multiplex knock-in, HEK293T cells were transfected with 200 ng of PE2 plasmid, 50 ng of each pegRNA plasmid DNA (four in total), 300 ng of Bxb1 plasmid DNA, and 150 ng of each DNA donor (two in total). Donor plasmid sequences can be found in Supplementary Sequences 1. The codon-optimized Bxb1 gene was purchased from Genscript and can be found in Supplementary Sequence 2. It was assembled into a pCMV expression vector using standard molecular cloning techniques.

For inversion experiments, sequential plasmid transfection and single-step mRNA nucleofection were performed. In the sequential plasmid transfection experiment, HEK293T cells were transfected with 750 ng of PE2 plasmid DNA, 62.5 ng of each pegRNA plasmid DNA (four in total) using Lipofectamine 2000 as described above. After three days, cells were detached and plated in 24-well plates, then serially passaged for about seven days. 48-well plates were seeded with 20,000 cells per well and transfected 16-24 h later with Lipofectamine 2000 and 500 ng of BxB1 plasmid DNA. Genomic DNA was extracted and prepared for Illumina MiSeq as described above. For single-step mRNA nucleofection, 200,000 HEK293T cells were nucleofected with 1,000 ng of PE2 mRNA, 30 pmol each of synthetic pegRNAs (4 pegRNAs in total), and 750 ng of BxB1 mRNA using 20 µL of Lonza buffer and cells with program CM-130. Cells were recovered with 80 µL of pre-warmed (37 °C) media for five minutes. 25-µL samples from the nucleofection cuvette were then added

to each well of the 48-well plate and incubated at 37 °C for 72 hours prior to isolation of genomic DNA as described above.

Droplet digital PCR analysis of knock-in efficiency.

Genomic DNA from crude cell lysates was column purified (Zymo) and DNA concentrations were determined by Nanodrop (Thermo Scientific). Droplet digital PCR was used to determine the abundance of an amplicon containing the genome-donor junction in comparison to a reference gene (*ACTB*). 100-200 ng of DNA was added to a reaction mixture containing ddPCR Supermix for Probes (Bio-Rad, 1863026), HindIII-HF (0.25 units/ μ L, New England BioLabs, R3104L), *ACTB* primers and probes (Supplementary Table 3; 900 nM each primer, 250 nM probe) and genome-donor junction primers and probes (Supplementary Table 3; 900 nM each primer, 250 nM probe) according to the manufacturer's protocol. Droplets were generated using a QX200 Manual Droplet Generator (Bio-Rad, 186-4002). Digital droplet PCR was performed as follows: 95 °C for 10 min, then 50 cycles of 94 °C for 30 seconds, 58 °C for 2 min. Following PCR cycles, a final incubation was conducted at 98 °C for 10 min. Droplets were read on a QX200 Droplet Reader (Bio-Rad, 1864001) using QuantaSoft (v. 1.4, Bio-Rad). Data were analyzed using QuantaSoft (v. 1.4, Bio-Rad).

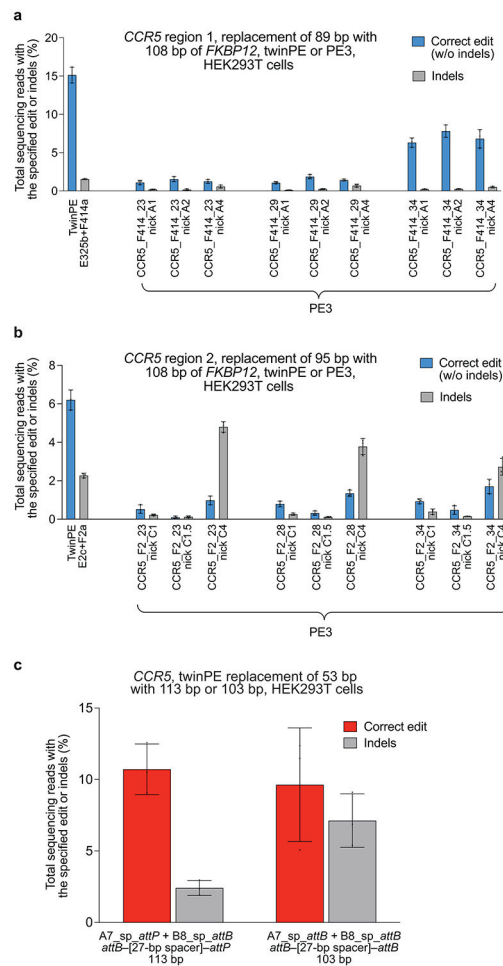
FIX expression from ALB locus in Huh7 cells.

Huh7 cells were transfected with 160 ng of Bxb1 plasmid DNA, 160 ng of donor plasmid DNA (*attP*-splice acceptor-cDNA of *F9* exons 2-8), 400 ng of prime editor plasmid DNA, and pegRNAs plasmid DNA for installation of *attB* in the first intron of *ALB* or at *CCR5* (40 ng each). Three days post-transfection, cells were passaged and allowed to grow to confluence. Their media was changed, and they were left to condition the fresh media, with aliquots taken at days 4, 7, and 10. Factor IX concentration in conditioned media was measured by ELISA (Innovative Research Human Total Factor IX ELISA Kit, IHUFIXKTT).

Lentivirus production, GFP reporter cell line construction, and flow cytometry analysis.

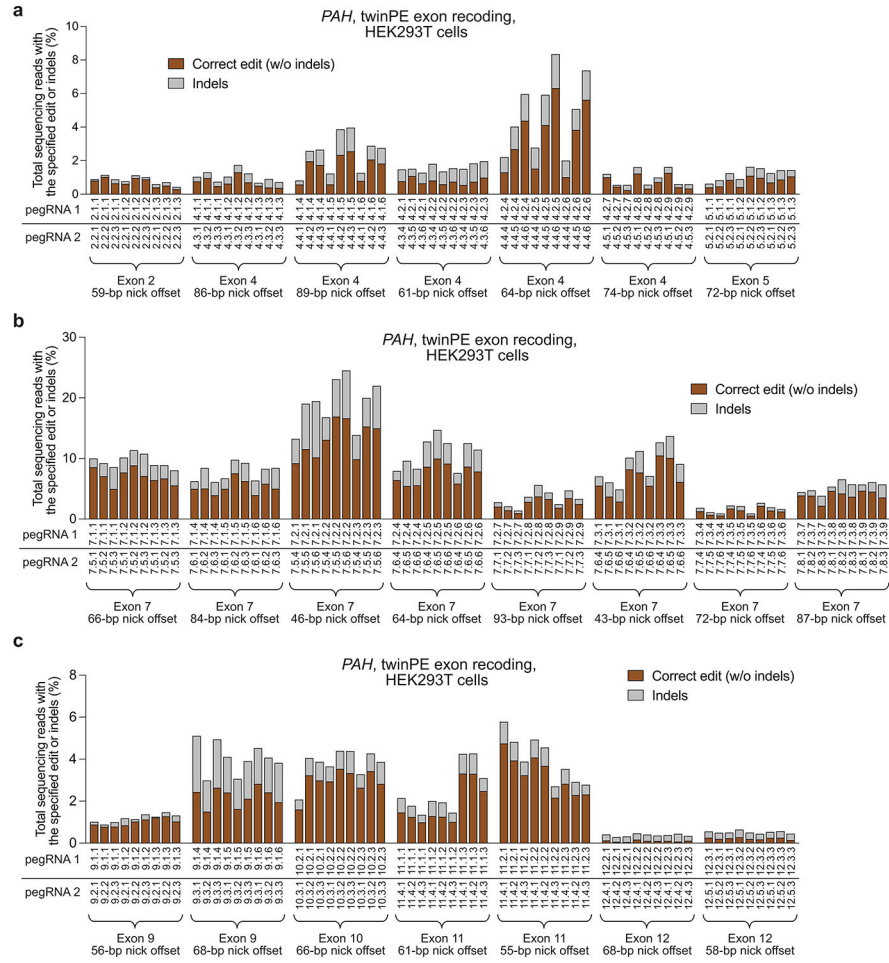
The lentiviral transfer vector described in Extended Data Figure 9 and Supplementary Sequence 3 was assembled using standard molecular cloning techniques. The lentivirus was produced as previously described^{6,7}. Briefly, a T-75 flask of rapidly dividing HEK293T cells (ATCC; Manassas, VA, USA) were transfected at 80-90% confluence with lentivirus helper plasmids pVSV-G and psPAX2 in along with the constructed lentiviral transfer vector using FuGENE HD (Promega) according to the manufacturer's protocol. After 48 hours, supernatant was collected, centrifuged at 3,000 x *g* for 15 minutes to remove cellular debris, and filtered using a 0.45- μ m PVDF filter. Filtered supernatant was concentrated using the PEG-it Virus Precipitation Solution (System Biosciences) according to the manufacturer's instructions. The resulting pellet was resuspended in Opti-MEM (Thermo Fisher Scientific) using 1% of the original medium volume. Resuspended pellet was used to transduce the HEK293T cells with multiplicity of infection. Successfully transduced cells that had stable GFP reporter integration were selected with 2.5 μ g/mL puromycin for more than 3 passages and then seeded into 48-well plates for transfection with PE2 plasmid DNA (750 ng), four *AAVS1*-targeting pegRNAs (62.5 ng each) for multiplexed *attP* and *attB* insertion, and Bxb1

Extended Data

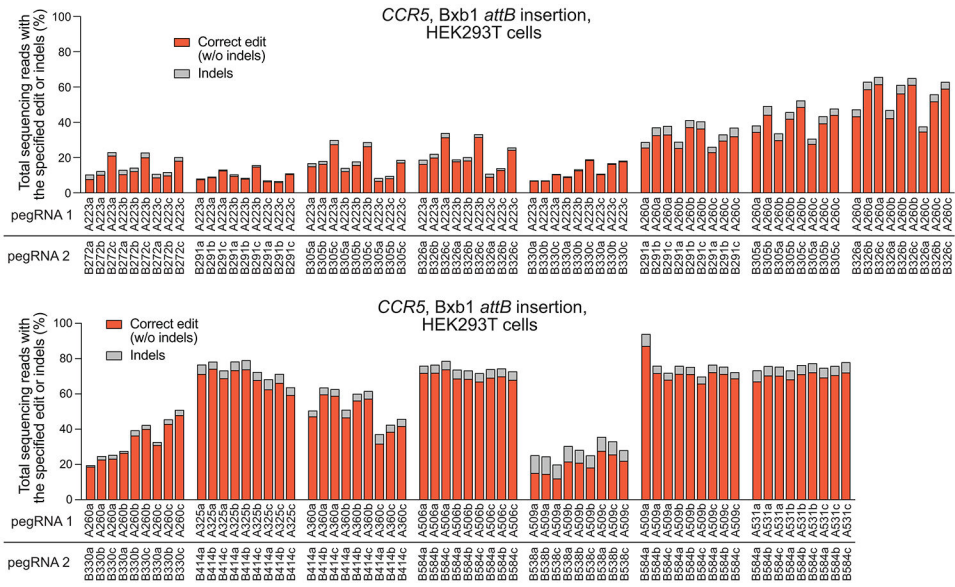


Extended Data Fig. 1. Twin prime editing mediates sequence replacements at *CCR5*
(a) Replacement of endogenous sequence within *CCR5* region 1 with a 108-bp fragment of *FKBP12* cDNA using twinPE (*FKBP12* sequence oriented in the forward direction,) or PE3 (*FKBP12* sequence oriented in the reverse direction). For PE3 editing, pegRNA RT templates were designed to encode 108 base pairs of *FKBP12* cDNA sequence and one of three different target-site homology sequence lengths. For PE3 edits, each pegRNA was tested with three nicking sgRNAs. **(b)** Replacement of endogenous sequence within *CCR5* region 2 with a 108-bp fragment of *FKBP12* cDNA sequence using twinPE (*FKBP12* sequence oriented in the forward direction) or PE3 (*FKBP12* sequence oriented in the reverse direction). As in (a), PE3 edits were tested with pegRNAs containing RT templates that were designed to encode 108 base pairs of *FKBP12* cDNA sequence and one of three different target-site homology sequence lengths. For PE3 edits, each pegRNA was tested with three nicking sgRNAs. Values and error bars reflect the mean and s.d. of three independent biological replicates. **(c)** Transfection of HEK293T cells with a pair of pegRNAs targeting *CCR5* leads to replacement of 53 base pairs of endogenous sequence with 113 base pairs (*attB*-[27-bp spacer]-*attP*) or 103 base pairs (*attB*-[27-bp spacer]-*attB*)

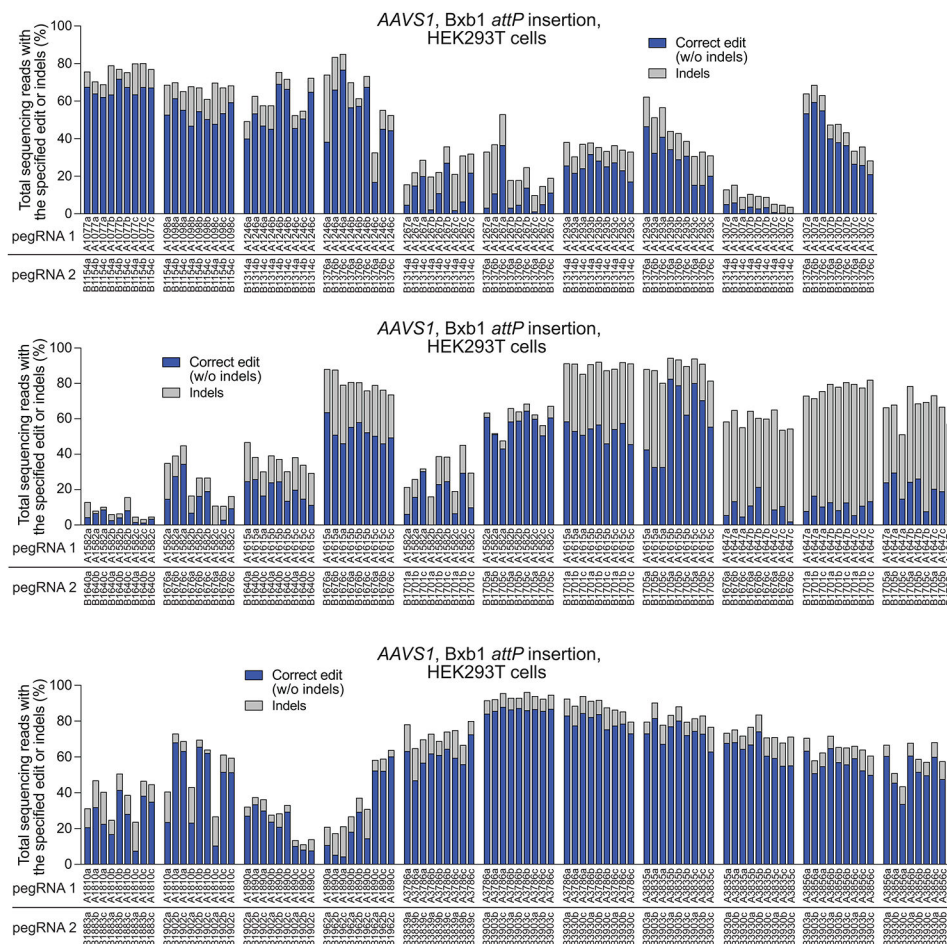
of exogenous sequence. Values and error bars reflect the mean and s.d. of three independent biological replicates.



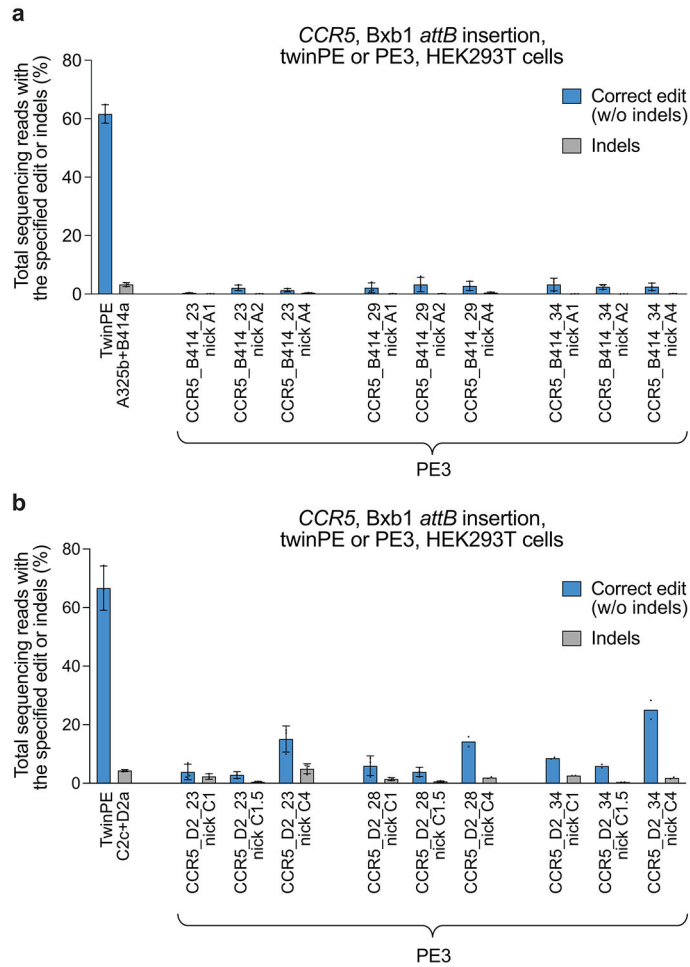
Extended Data Fig. 2. Recoding of PAH exon sequences in HEK293T cells via twinPE Screen of pегRNA pairs targeting PAH for recoding of (a) exons 2, 4 and 5, (b) exon 7, and (c) exons 9, 10, 11, and 12. RT templates of pегRNAs encoded partially recoded exonic sequence to optimize orthogonality to the endogenous gene sequence. For each spacer pair, nine pегRNA combinations were tested using three PBS variants for each spacer in a three-by-three matrix, with RT templates encoding the recoded exonic sequence, which was held constant for given spacer pairs. Sequences of pегRNAs are listed in Supplementary Table 1. Sequences of recoded exonic sequences are listed in Supplementary Table 4. Values in (a), (b) and exon 9 in (c) reflect single biological replicates. Values for exons 10, 11 and 12 in (c) reflect the mean of three independent biological replicates.



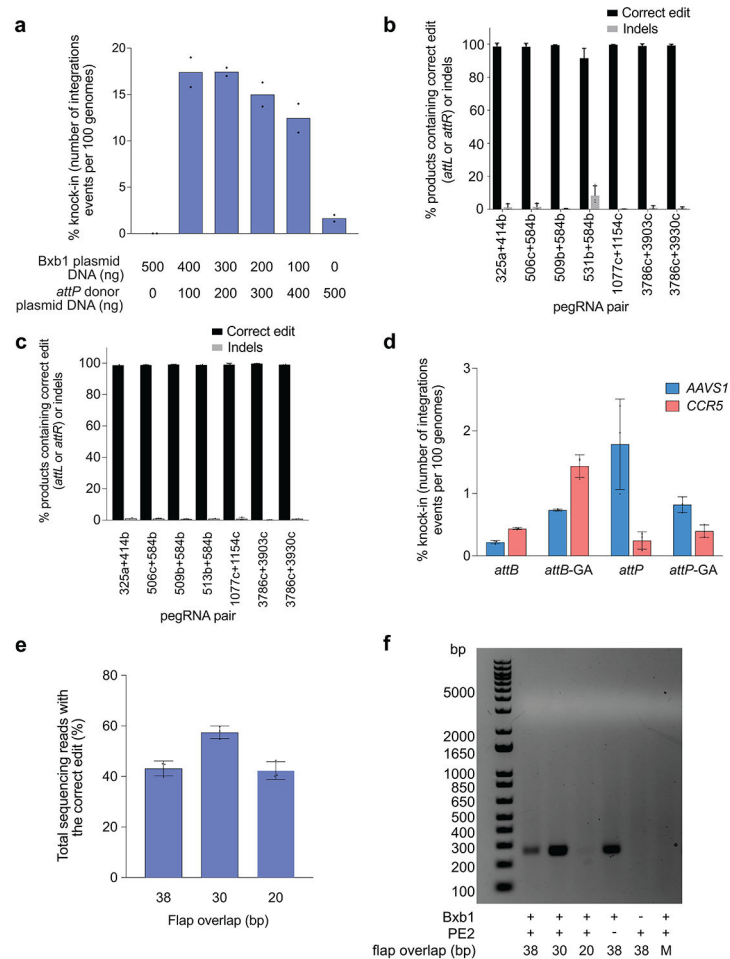
Extended Data Fig. 3. Installation of a 38-bp Bxb1 attB site at CCR5 with twinPE
 Spacer pairs targeting the *CCR5* locus were designed for twinPE-mediated insertion of the Bxb1 attB attachment site. For each spacer, three pegRNAs were designed having three different PBS lengths and a fixed RT template that encodes the full-length Bxb1 attB sequence (38 bp). Sequences of pegRNAs are listed in Supplementary Table 1. For each spacer pair, a three-by-three matrix of pegRNA combinations was tested by plasmid DNA co-transfection with PE2 in HEK293T cells. Each pegRNA pair is specified below the x-axis. Values reflect single biological replicates.



Extended Data Fig. 4. Installation of a 50-bp Bxb1 *attP* site at *AAVS1* with twinPE
 Spacer pairs targeting the *AAVS1* locus were designed for twinPE-mediated insertion of the Bxb1 *attP* attachment site. For each spacer, three pegRNAs were designed having three different PBS lengths and a fixed RT template that encodes a portion (43-44 bp) of the Bxb1 *attP* sequence. Sequences of pegRNAs are listed in Supplementary Table 1. For each spacer pair, a three-by-three matrix of pegRNA combinations was tested by plasmid DNA co-transfection with PE2 in HEK293T cells. Each pegRNA pair is specified below the x-axis. Values reflect single biological replicates.



Extended Data Fig. 5. Comparison of twinPE and PE3 for Bxb1 *attB* insertion at *CCR5*
(a) Replacement of endogenous sequence within *CCR5* region 1 with the Bxb1 *attB* site using twinPE or PE3. For PE3 editing systems, pegRNA RT templates were designed to encode the Bxb1 *attB* sequence and one of three different target-site homology sequence lengths. For PE3 edits, each pegRNA was tested with three nicking sgRNAs. **(b)** Replacement of endogenous sequence within *CCR5* region 2 with the Bxb1 *attB* sequence using twinPE or PE3. As in (a), PE3 edits were tested with pegRNAs containing RT templates that were designed to encode the Bxb1 *attB* sequence and one of three different target-site homology sequence lengths and tested with three nicking sgRNAs. Values and error bars in (a) and TwinPE edits, PE3 edits of *CCR5*D2_23, *CCR5*D2_28 with nicking guide RNA C1 and C1.5 in (b) reflect the mean and s.d. of three independent biological replicates. Values of *CCR5*D2_28 with nicking guide RNA C4 and *CCR5*D2_34 in (b) reflect the mean of two independent biological replicates.

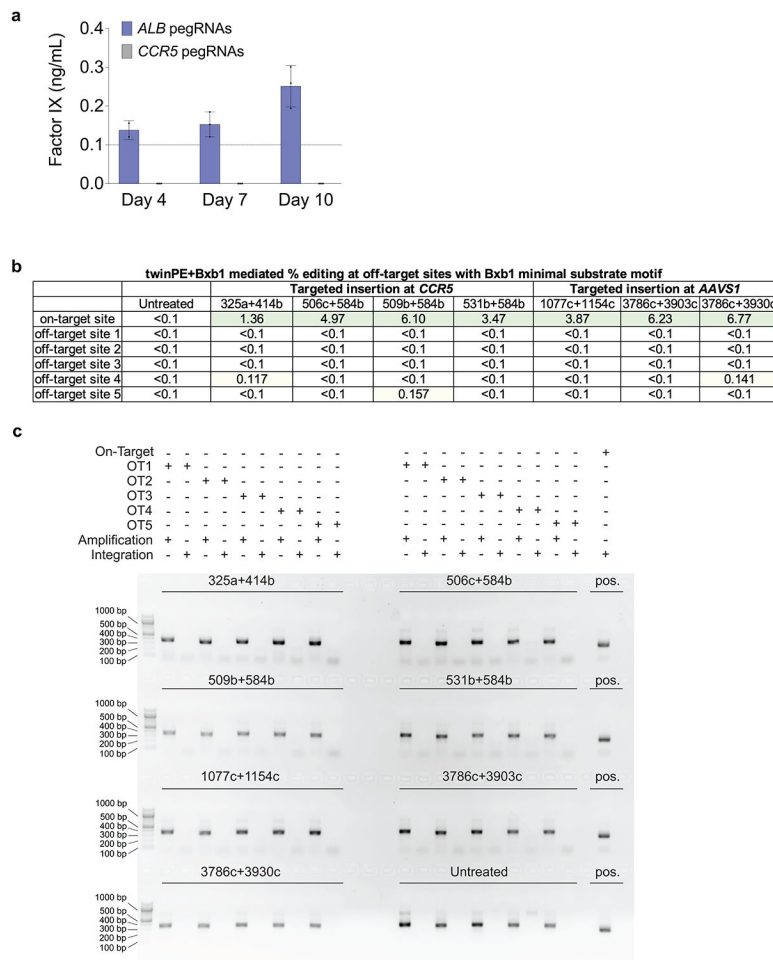


Extended Data Fig. 6. TwinPE combined with Bxb1 recombinase for targeted knock-in of donor DNA plasmids

(a) Bxb1-mediated DNA donor knock-in in clonal HEK293T cell lines. Transfection of a HEK293T clonal cell line containing homozygous *attB* site insertion at *CCR5* with varying amounts of Bxb1-expressing plasmid and *attP*-containing donor DNA plasmid. Knock-in efficiency was quantified by ddPCR. Values and error bars reflect the mean of two independent biological replicates. (b) Assessment of genome-donor junction purity by high-throughput sequencing. Genomic DNA from single-transfection knock-in experiments was amplified with a forward primer that binds the genome and a reverse primer that binds within the donor plasmid (Supplementary Table 2). Values and error bars reflect the mean and s.d. of three independent biological replicates. (c) Assessment of genome-donor junction purity at the other junction by high-throughput sequencing as performed in (b). Values and error bars in 506c+584b, 509b+584b, 1077c+1154c, and 3786c+3903c reflect the mean and s.d. of three independent biological replicates. Values in 325a+414b, 513b+584b, 3786c+3930c reflect the mean of two independent biological replicates. (d) Multiplexed single-transfection knock-in at *AAVS1* and *CCR5*. HEK293T cells were transfected with plasmids encoding PE2, Bxb1, a pair of pegRNAs for the insertion of *attP* at *AAVS1*, an *attB*-donor, a pegRNA pair for the insertion of one of four attachment sites (*attB*, *attB-GA*, *attP*, or *attP-GA*) at *CCR5*, and a corresponding donor. Knock-in was observed

at both target loci under all four conditions. Insertion of *attP* at *AAVS1* and *attB* at *CCR5* gave the lowest knock-in efficiencies overall (0.2% at *AAVS1*, 0.4% at *CCR5*). Insertion of *attP* at both sites yielded the highest levels of knock-in at *AAVS1* (1.8%) but low levels (0.2%) at *CCR5*. When an orthogonal edit (*attB*-GA or *attP*-GA) was introduced at *CCR5*, *AAVS1* knock-in was 0.7-0.8%. Higher knock-in at *CCR5* was observed with *attB*-GA (1.4%) than with *attP*-GA (0.4%), consistent with our single locus knock-in results. Values and error bars reflect the mean and s.d. of three independent biological replicates.

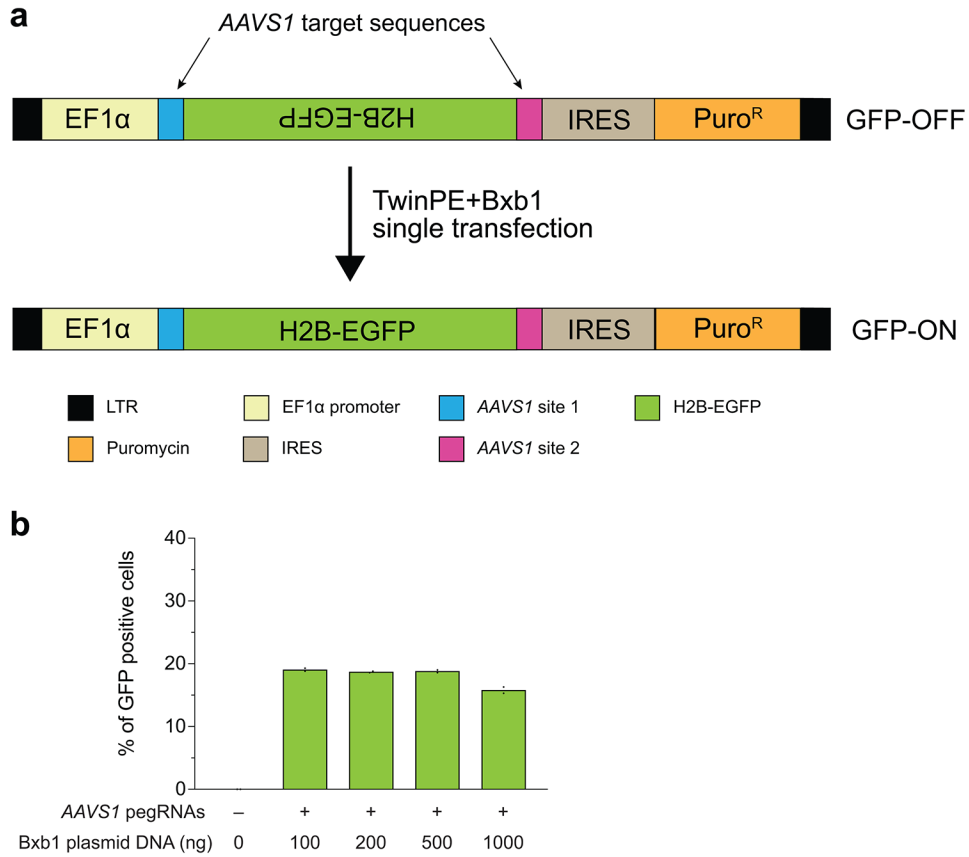
(e) and **(f)** Effects of reducing pegRNA overlap on twinPE efficiency and donor/pegRNA recombination. **(e)** The editing efficiencies of pairs of pegRNAs for insertion of Bxb1 *attB* at *CCR5* were measured by high-throughput sequencing. The pairs differed in the amount of overlap shared between their flaps, from 38 bp (full-length *attB* sequence) down to 20 bp. Editing efficiency of the pairs with shorter overlaps was comparable to the pair with full-length overlap. Values and error bars reflect the mean and s.d. of three independent biological replicates. **(f)** Assessment of recombination between *attB*-containing pegRNA plasmids and *attP*-containing donor plasmids. Following transfection of HEK293T cells with the indicated samples, isolated DNA was amplified with a forward primer that binds the pegRNA expression plasmid (TTGAAAAAGTGGCACCGAGT) and a reverse primer that binds the donor plasmid (CTCCCACTCATGATCTA). A positive 256-bp PCR band confirms recombination between the two plasmids. When the pegRNA encodes full-length *attB* (38-bp) or a truncated version of *attB* with 30-bp of overlap between flaps, a band is observed; however, recombination is not observed when the pegRNAs encode a truncated *attB* with only 20-bp of flap overlap. The “No PE2” control uses the 38-bp overlap pegRNA pair. No recombination is observed in the absence of Bxb1 or if the donor and pegRNA plasmids both bear *attB* (Mismatch, “M”). Three independent biological replicates were performed and a representative image from one of the replicates is shown.



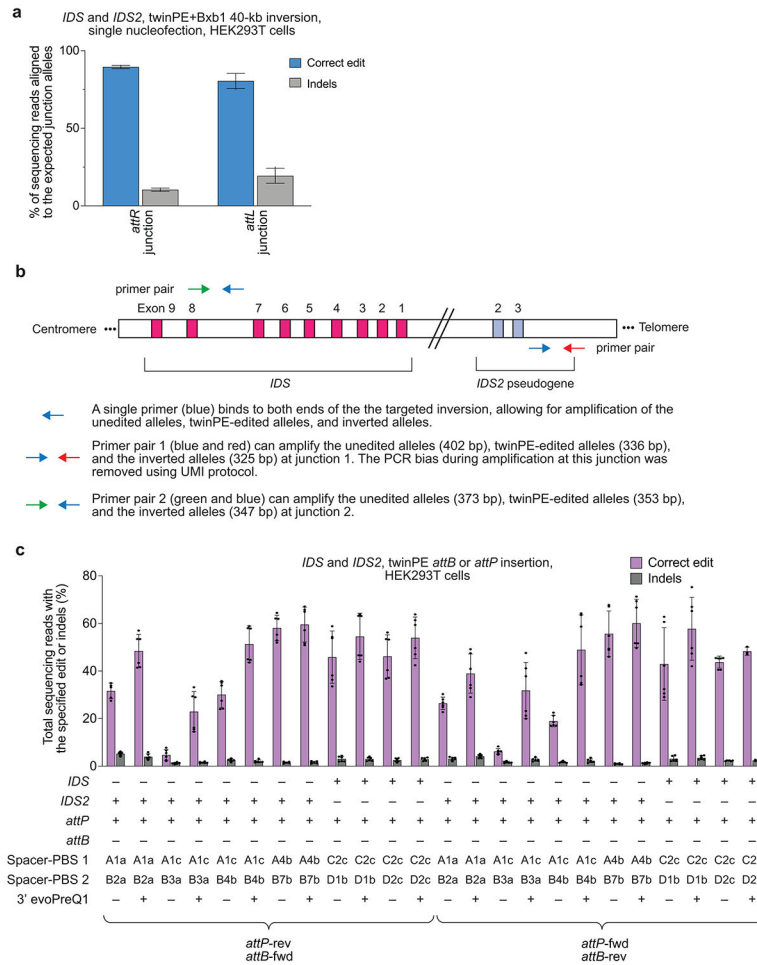
Extended Data Fig. 7. Expression of human Factor IX from the ALB promoter following twinPE-recombinase knock-in and characterization of Bxb1 off-target editing

(a) Huh7 cells were transfected with Bxb1, donor (*attP*-splice acceptor-cDNA of *F9* exons 2-8), PE2, and pegRNAs for installation of *attB* in the first intron of *ALB* or at *CCR5*. Three days post-transfection, cells were split and allowed to grow to confluence. Their media was changed, and they were left to condition the fresh media, with aliquots taken at days 4, 7, and 10. Factor IX was present at detectable levels by ELISA (dashed line represents the lower limit of detection) in two of three samples treated with *ALB* pegRNAs at Day 4, and in all samples treated with *ALB* pegRNAs at Day 7 and Day 10. Factor IX was never detected in the conditioned media of any samples treated with *CCR5* pegRNAs. Values and error bars reflect the mean and s.d. of two or three independent biological replicates. (b) Targeted amplicon sequencing was performed for each of the five nominated pseudo-sites (OT1-OT5) from seven different samples treated with 5.6-kb donor DNA plasmid, twinPE reagents targeting *CCR5* or *AAVS1*, and Bxb1 recombinase. The indels in all five pseudo-sites are either below the limit of detection (<0.1%) or near-background compared to untreated controls. The integration efficiency at the on-target site was measured by ddPCR as shown in Fig. 3d (c) To capture potential donor plasmid integration events at nominated pseudo-sites, primers were used to amplify predicted integration junctions. The gel depicts PCR reactions performed for each off-target site as indicated in the above legend.

Confirmation of on-target donor integration from the samples is shown in the right-most column of the gel. In (b) and (c), two or three independent biological replicates were performed.

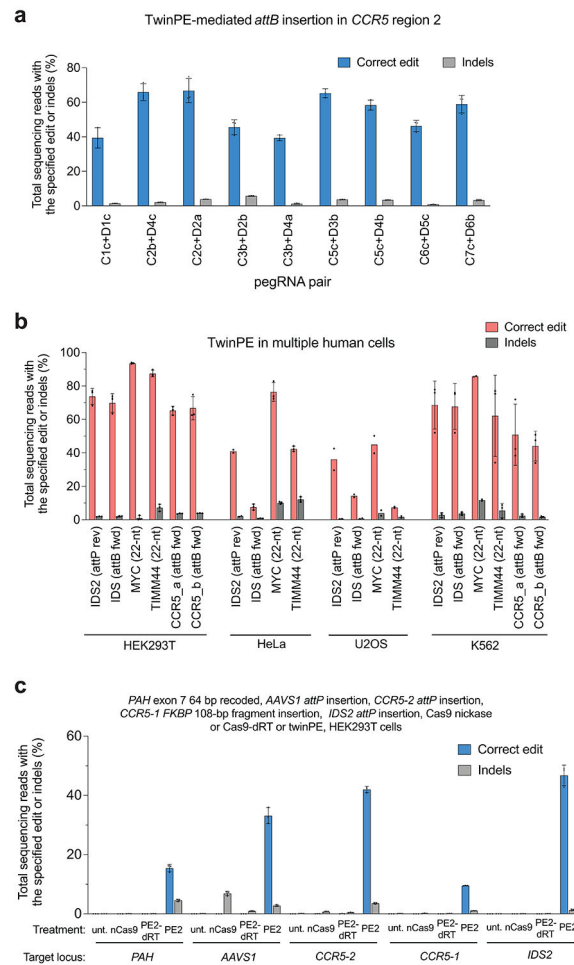


Extended Data Fig. 8. TwinPE and Bxb1-mediated inversion in HEK293T GFP reporter cells
(a) The lentiviral fluorescent reporter construct used to assess inversion efficiency with twinPE and Bxb1 recombinase. The reporter contains an EF1 α promoter followed by an inverted H2B-EGFP coding sequence that is flanked by partial *AAVS1* DNA sequence, an internal ribosome entry site (IRES), and a puromycin resistance gene. Successful installation of opposite-facing *attB* (left) and *attP* (right) sequences at the *AAVS1* target sequences and subsequent inversion by Bxb1 corrects the orientation of GFP for functional expression. **(b)** The fluorescent reporter construct was stably integrated into HEK293T cells via lentiviral transduction and puromycin selection. The polyclonal GFP reporter cell line was then transfected with twinPE plasmid components (PE2 and four pegRNAs) and varying amounts of Bxb1 plasmid for single-transfection inversion. Cells were analyzed by flow cytometry and gated for live single cells. Quantification of GFP positive cells by flow cytometry. Values and error bars reflect the mean of two independent biological replicates.



Extended Data Fig. 9. TwinPE and Bxb1 recombinase-mediated inversion between *IDS* and *IDS2*

(a) Assessment of the inverted *IDS* junction purity by high-throughput sequencing in HEK293T cells. Frequency of expected junction sequences containing *attR* and *attL* recombination products after twinPE and BxB1-mediated single-step inversion. The product purities range from 81-89%. Values and error bars reflect the mean and s.d. of three independent biological replicates. **(b)** Schematic diagram of the designed PCR strategies for quantifying *IDS* inversion efficiency. Primer pair 1 (green forward and blue reverse primer) can amplify the unedited alleles (403 bp), twinPE-edited alleles (337 bp), and the inverted alleles (326 bp) at junction 1 in a single PCR reaction. Due to the size difference, a UMI protocol was applied to eliminate PCR bias during quantification of inversion efficiency. Similarly, using primer pair 2 (red forward and blue reverse primer), the unedited alleles (346 bp), twinPE-edited alleles (326 bp), and inverted alleles (320 bp) at junction 2 can be amplified in a single PCR reaction. Amplicons can then be sequenced by standard high-throughput sequencing protocols for amplicon sequencing. **(c)** Screening of pegRNA pairs for the insertion of Bxb1 *attB* and *attP* sequences at *IDS* and *IDS2*. TwinPE editing was tested with standard pegRNAs and epegRNAs containing a 3' evoPreQ1 motif. Values and error bars reflect the mean and s.d. of three independent biological replicates.



Extended Data Fig. 10. Twin prime editing mediated insertion in *CCR5* region 2 in HEK293T cells, twin prime editing in multiple human cell lines, and editing activity of Cas9 nickase and PE2-dead RT variants

(a) TwinPE-mediated endogenous sequence replacement with Bxb1 *attB* attachment site in *CCR5* region 2 in HEK293T cells. (b) TwinPE-mediated endogenous sequence replacement with *attP*, *attB*, or 22-nt DNA sequences in multiple human cell lines. Six different pegRNA pairs targeting five loci were tested in HEK293T, HeLa, U2OS and K562 cells. HEK293T and HeLa cell were transfected with PE2 and pegRNA plasmids via Lipofectamine 2000 (Thermo Fisher) and *TransIT-HeLaMonster* (Mirus), respectively. U2OS and K562 cells were nucleofected using Lonza 4D-Nucleofector and SE kit. DNA loci and the specified insertion edits are shown in the x-axis. (c) HEK293T cells were transfected with twinPE pegRNA pairs and either Cas9–H840A nickase (nCas9), PE2-dRT (a PE2 variant that contains K103L and R110S inactivating mutations to the RT domain), or PE2. Treatment with either nCas9 or PE2-dRT did not result in desired edits, while PE2 installed the specified edits as indicated. Values and error bars in (a) and (c) reflect the mean and s.d. of three independent biological replicates. Values and error bars in (b) reflect the mean and s.d. of at least two independent biological replicates except editing in *IDS2* in HeLa cells, editing in U2OS cells, and editing in *MYC* in K562 cells, which represent two independent biological replicates.

Supplementary Material

Refer to Web version on PubMed Central for supplementary material.

Acknowledgements

We thank Erik Sontheimer's group for sharing Huh7 cells and Liu Lab members for helpful discussions. This work was supported by the Merkin Institute of Transformative Technologies in Healthcare, US NIH grants U01 AI142756, RM1 HG009490, and R35 GM118062, and the HHMI. A.V.A. acknowledges a Jane Coffin Childs postdoctoral fellowship through the HHMI.

Data availability

High-throughput sequencing data have been deposited to the NCBI Sequence Read Archive database under accession PRJNA770428. Droplet digital PCR, flow cytometry, and hFIX ELISA data available upon request.

References

1. Auton A et al. A global reference for human genetic variation. *Nature* 526, 68–74, doi:10.1038/nature15393 (2015). [PubMed: 26432245]
2. Landrum MJ et al. ClinVar: public archive of relationships among sequence variation and human phenotype. *Nucleic Acids Res* 42, D980–985, doi:10.1093/nar/gkt1113 (2014). [PubMed: 24234437]
3. Weischenfeldt J, Symmons O, Spitz F & Korbel JO Phenotypic impact of genomic structural variation: insights from and for human disease. *Nat Rev Genet* 14, 125–138, doi:10.1038/nrg3373 (2013). [PubMed: 23329113]
4. Cox DB, Platt RJ & Zhang F Therapeutic genome editing: prospects and challenges. *Nat Med* 21, 121–131, doi:10.1038/nm.3793 (2015). [PubMed: 25654603]
5. Doudna JA The promise and challenge of therapeutic genome editing. *Nature* 578, 229–236, doi:10.1038/s41586-020-1978-5 (2020). [PubMed: 32051598]
6. Anzalone AV, Koblan LW & Liu DR Genome editing with CRISPR-Cas nucleases, base editors, transposases and prime editors. *Nat Biotechnol* 38, 824–844, doi:10.1038/s41587-020-0561-9 (2020). [PubMed: 32572269]
7. Jinek M et al. A Programmable Dual-RNA-Guided DNA Endonuclease in Adaptive Bacterial Immunity. *Science* 337, 816–821, doi:10.1126/science.1225829 (2012). [PubMed: 22745249]
8. Cong L et al. Multiplex genome engineering using CRISPR/Cas systems. *Science (New York, N.Y.)* 339, 819–823, doi:10.1126/science.1231143 (2013).
9. Mali P et al. RNA-guided human genome engineering via Cas9. *Science* 339, 823–826, doi:10.1126/science.1232033 (2013). [PubMed: 23287722]
10. Komor AC, Kim YB, Packer MS, Zuris JA & Liu DR Programmable editing of a target base in genomic DNA without double-stranded DNA cleavage. *Nature* 533, 420–424, doi:10.1038/nature17946 (2016). [PubMed: 27096365]
11. Gaudelli NM et al. Programmable base editing of A*T to G*C in genomic DNA without DNA cleavage. *Nature* 551, 464–471, doi:10.1038/nature24644 (2017). [PubMed: 29160308]
12. Anzalone AV et al. Search-and-replace genome editing without double-strand breaks or donor DNA. *Nature* 576, 149–157, doi:10.1038/s41586-019-1711-4 (2019). [PubMed: 31634902]
13. Canver MC et al. Characterization of genomic deletion efficiency mediated by clustered regularly interspaced short palindromic repeats (CRISPR)/Cas9 nuclease system in mammalian cells. *The Journal of biological chemistry* 289, 21312–21324, doi:10.1074/jbc.M114.564625 (2014). [PubMed: 24907273]
14. Suzuki K et al. In vivo genome editing via CRISPR/Cas9 mediated homology-independent targeted integration. *Nature* 540, 144–149, doi:10.1038/nature20565 (2016). [PubMed: 27851729]

15. Wang B et al. Highly efficient CRISPR/HDR-mediated knock-in for mouse embryonic stem cells and zygotes. *Biotechniques* 59, 201–202, 204, 206–208, doi:10.2144/000114339 (2015). [PubMed: 26458548]
16. Pawelczak KS, Gavande NS, VanderVere-Carozza PS & Turchi JJ Modulating DNA Repair Pathways to Improve Precision Genome Engineering. *ACS Chem Biol* 13, 389–396, doi:10.1021/acscchembio.7b00777 (2018). [PubMed: 29210569]
17. Branzei D & Foiani M Regulation of DNA repair throughout the cell cycle. *Nature Reviews Molecular Cell Biology* 9, 297–308, doi:10.1038/nrm2351 (2008). [PubMed: 18285803]
18. Heyer WD, Ehmsen KT & Liu J Regulation of homologous recombination in eukaryotes. *Annual review of genetics* 44, 113–139, doi:10.1146/annurev-genet-051710-150955 (2010).
19. Gasperini M et al. CRISPR/Cas9-mediated scanning for regulatory elements required for HPRT1 expression via thousands of large, programmed genomic deletions. *The American Journal of Human Genetics* 101, 192–205 (2017). [PubMed: 28712454]
20. Kosicki M, Tomberg K & Bradley A Repair of double-strand breaks induced by CRISPR–Cas9 leads to large deletions and complex rearrangements. *Nature Biotechnology* 36, 765–771, doi:10.1038/nbt.4192 (2018).
21. Alanis-Lobato G et al. Frequent loss-of-heterozygosity in CRISPR–Cas9–edited early human embryos. *Proceedings of the National Academy of Sciences*, 202004832, doi:10.1073/pnas.2004832117 (2021).
22. Song Y et al. Large-Fragment Deletions Induced by Cas9 Cleavage while Not in the BEs System. *Molecular Therapy - Nucleic Acids* 21, 523–526, doi:10.1016/j.omtn.2020.06.019 (2020). [PubMed: 32711379]
23. Brunet E & Jasin M Induction of Chromosomal Translocations with CRISPR–Cas9 and Other Nucleases: Understanding the Repair Mechanisms That Give Rise to Translocations. *Advances in experimental medicine and biology* 1044, 15–25, doi:10.1007/978-981-13-0593-1_2 (2018). [PubMed: 29956288]
24. Nahmad AD et al. Frequent Aneuploidy in Primary Human T Cells Following CRISPR–Cas9 cleavage. *bioRxiv*, 2021.2008.2020.457092, doi:10.1101/2021.08.20.457092 (2021).
25. Leibowitz ML et al. Chromothripsis as an on-target consequence of CRISPR–Cas9 genome editing. *Nature Genetics*, doi:10.1038/s41588-021-00838-7 (2021).
26. Haapaniemi E, Botla S, Persson J, Schmierer B & Taipale J CRISPR–Cas9 genome editing induces a p53-mediated DNA damage response. *Nature Medicine* 24, 927–930, doi:10.1038/s41591-018-0049-z (2018).
27. Ihry RJ et al. p53 inhibits CRISPR–Cas9 engineering in human pluripotent stem cells. *Nature Medicine* 24, 939–946, doi:10.1038/s41591-018-0050-6 (2018).
28. Enache OM et al. Cas9 activates the p53 pathway and selects for p53-inactivating mutations. *Nat Genet* 52, 662–668, doi:10.1038/s41588-020-0623-4 (2020). [PubMed: 32424350]
29. Merrick CA, Zhao J & Rosser SJ Serine Integrases: Advancing Synthetic Biology. *ACS Synthetic Biology* 7, 299–310, doi:10.1021/acssynbio.7b00308 (2018). [PubMed: 29316791]
30. Karpinski J et al. Directed evolution of a recombinase that excises the provirus of most HIV-1 primary isolates with high specificity. *Nat Biotechnol* 34, 401–409, doi:10.1038/nbt.3467 (2016). [PubMed: 26900663]
31. Chaikind B, Bessen JL, Thompson DB, Hu JH & Liu DR A programmable Cas9-serine recombinase fusion protein that operates on DNA sequences in mammalian cells. *Nucleic Acids Res* 44, 9758–9770, doi:10.1093/nar/gkw707 (2016). [PubMed: 27515511]
32. Gaj T et al. Enhancing the Specificity of Recombinase-Mediated Genome Engineering through Dimer Interface Redesign. *J Am Chem Soc* 136, 5047–5056, doi:10.1021/ja4130059 (2014). [PubMed: 24611715]
33. Kim AI et al. Mycobacteriophage Bxb1 integrates into the *Mycobacterium smegmatis* groEL1 gene. *Molecular Microbiology* 50, 463–473, doi:10.1046/j.1365-2958.2003.03723.x (2003). [PubMed: 14617171]
34. Choi J et al. Precise genomic deletions using paired prime editing. *Nat Biotechnol*, doi:10.1038/s41587-021-01025-z (2021).

35. Lin Q et al. High-efficiency prime editing with optimized, paired pegRNAs in plants. *Nature Biotechnology*, doi:10.1038/s41587-021-00868-w (2021).
36. Scriver CR The PAH gene, phenylketonuria, and a paradigm shift. *Human Mutation* 28, 831–845, doi:10.1002/humu.20526 (2007). [PubMed: 17443661]
37. Nelson JW et al. Engineered pegRNAs improve prime editing efficiency. *Nat Biotechnol*, doi:10.1038/s41587-021-01039-7 (2021).
38. Flanigan KM et al. Mutational spectrum of DMD mutations in dystrophinopathy patients: application of modern diagnostic techniques to a large cohort. *Human mutation* 30, 1657–1666, doi:10.1002/humu.21114 (2009). [PubMed: 19937601]
39. Aartsma-Rus A et al. Development of Exon Skipping Therapies for Duchenne Muscular Dystrophy: A Critical Review and a Perspective on the Outstanding Issues. *Nucleic acid therapeutics* 27, 251–259, doi:10.1089/nat.2017.0682 (2017). [PubMed: 28796573]
40. Kim DY, Moon SB, Ko J-H, Kim Y-S & Kim D Unbiased investigation of specificities of prime editing systems in human cells. *Nucleic Acids Research* 48, 10576–10589, doi:10.1093/nar/gkaa764 (2020). [PubMed: 32941652]
41. Jin S et al. Genome-wide specificity of prime editors in plants. *Nature Biotechnology*, doi:10.1038/s41587-021-00891-x (2021).
42. Duportet X et al. A platform for rapid prototyping of synthetic gene networks in mammalian cells. *Nucleic acids research* 42, 13440–13451, doi:10.1093/nar/gku1082 (2014) [PubMed: 25378321]
43. Jusiak B et al. Comparison of Integrases Identifies Bxb1-GA Mutant as the Most Efficient Site-Specific Integrase System in Mammalian Cells. *ACS Synthetic Biology* 8, 16–24, doi:10.1021/acssynbio.8b00089 (2019). [PubMed: 30609349]
44. Sharma R et al. In vivo genome editing of the albumin locus as a platform for protein replacement therapy. *Blood* 126, 1777–1784, doi:10.1182/blood-2014-12-615492
45. Nathwani AC et al. Long-Term Safety and Efficacy of Factor IX Gene Therapy in Hemophilia B. *New Engl J Med* 371, 1994–2004, doi:10.1056/NEJMoa1407309 (2014). [PubMed: 25409372]
46. Bessen JL et al. High-resolution specificity profiling and off-target prediction for site-specific DNA recombinases. *Nature Communications* 10, 1937, doi:10.1038/s41467-019-09987-0 (2019).
47. Bondeson ML et al. Inversion of the IDS gene resulting from recombination with IDS-related sequences is a common cause of the Hunter syndrome. *Human molecular genetics* 4, 615–621, doi:10.1093/hmg/4.4.615 (1995). [PubMed: 7633410]
48. Chen X et al. In trans paired nicking triggers seamless genome editing without double-stranded DNA cutting. *Nat Commun* 8, 657, doi:10.1038/s41467-017-00687-1 (2017). [PubMed: 28939824]
49. Park CY et al. Targeted inversion and reversion of the blood coagulation factor 8 gene in human iPS cells using TALENs. *Proc Natl Acad Sci U S A* 111, 9253–9258, doi:10.1073/pnas.1323941111 (2014). [PubMed: 24927536]
50. Li J et al. Efficient inversions and duplications of mammalian regulatory DNA elements and gene clusters by CRISPR/Cas9. *Journal of molecular cell biology* 7, 284–298, doi:10.1093/jmcb/mjv016 (2015). [PubMed: 25757625]

Methods References

1. Anzalone AV et al. Search-and-replace genome editing without double-strand breaks or donor DNA. *Nature* 576, 149–157, doi:10.1038/s41586-019-1711-4 (2019). [PubMed: 31634902]
2. Komor AC, Kim YB, Packer MS, Zuris JA & Liu DR Programmable editing of a target base in genomic DNA without double-stranded DNA cleavage. *Nature* 533, 420–424, doi:10.1038/nature17946 (2016). [PubMed: 27096365]
3. Clement K et al. CRISPResso2 provides accurate and rapid genome editing sequence analysis. *Nature Biotechnology* 37, 224–226, doi:10.1038/s41587-019-0032-3 (2019).
4. Clement K, Farouni R, Bauer DE & Pinello L AmpUMI: design and analysis of unique molecular identifiers for deep amplicon sequencing. *Bioinformatics* 34, i202–i210, doi:10.1093/bioinformatics/bty264 (2018). [PubMed: 29949956]

5. Shen W, Le S, Li Y & Hu F SeqKit: A Cross-Platform and Ultrafast Toolkit for FASTA/Q File Manipulation. *PLoS One* 11, e0163962, doi:10.1371/journal.pone.0163962 (2016). [PubMed: 27706213]
6. Levy JM & Nicoll RA Membrane-associated guanylate kinase dynamics reveal regional and developmental specificity of synapse stability. *The Journal of Physiology* 595, 1699–1709, doi:10.1113/JP273147 (2017). [PubMed: 27861918]
7. Koblan LW et al. In vivo base editing rescues Hutchinson–Gilford progeria syndrome in mice. *Nature* 589, 608–614, doi:10.1038/s41586-020-03086-7 (2021). [PubMed: 33408413]
8. Gaudelli NM et al. Directed evolution of adenine base editors with increased activity and therapeutic application. *Nature Biotechnology* 38, 892–900, doi:10.1038/s41587-020-0491-6 (2020).
9. Nelson JW et al. Engineered pegRNAs improve prime editing efficiency. *Nat Biotechnol*, doi:10.1038/s41587-021-01039-7 (2021).

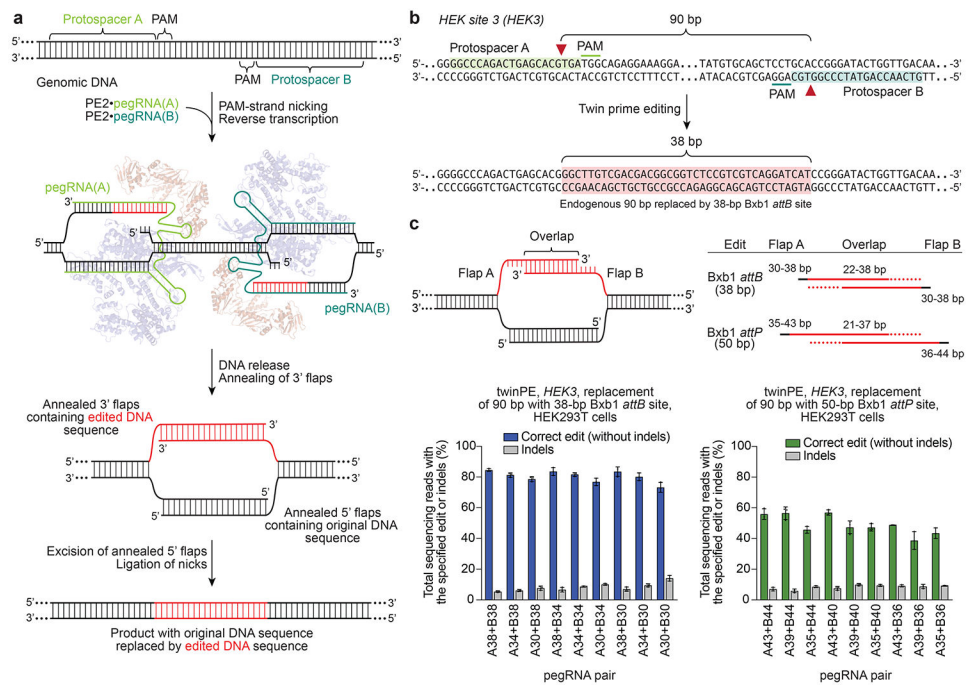


Figure 1 | Overview of twinPE and twinPE-mediated sequence replacement.

(a) TwinPE systems target genomic DNA sequences that contain two protospacer sequences on opposite strands of DNA. PE2•pegRNA complexes target each protospacer, generate a single-stranded nick, and reverse transcribe the pegRNA-encoded template containing the desired insertion sequence. After synthesis and release of the 3' DNA flaps, a hypothetical intermediate exists possessing annealed 3' flaps containing the edited DNA sequence and annealed 5' flaps containing the original DNA sequence. Excision of the original DNA sequence contained in the 5' flaps, followed by ligation of the 3' flaps to the corresponding excision sites, generates the desired edited product. (b) Example of twinPE-mediated replacement of a 90-bp sequence in *HEK3* with a 38-bp Bxb1 *attB* sequence. Red arrows indicate the position of pegRNA-induced nicks. (c) Evaluation of twinPE in HEK293T cells for the installation of the 38-bp Bxb1 *attB* site as shown in (b) or the 50-bp Bxb1 *attP* site at *HEK3* using pegRNAs that template varying lengths of the insertion sequence. pegRNA names indicate spacer (A or B) and length of RT template. Values and error bars reflect the mean and s.d. of three independent biological replicates.

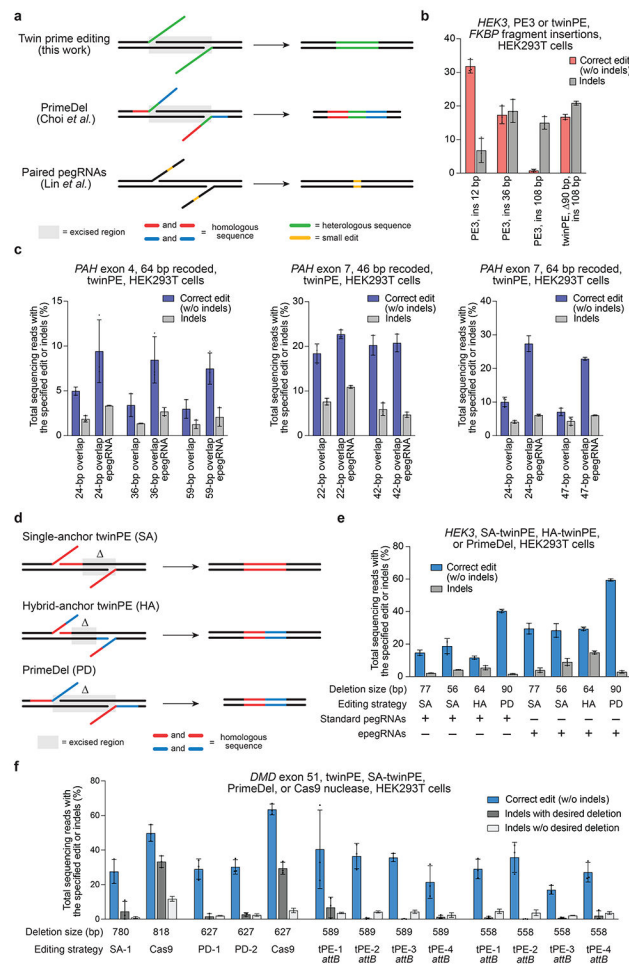


Figure 2 | Targeted sequence insertion, deletion, and recoding with twinPE in human cells. (a) Schematic diagram illustrating designs and edits generated for twinPE, PrimeDel³⁶ and paired pegRNAs³⁷. Shaded gray boxes indicate regions where DNA is excised, green lines indicate the incorporation of heterologous DNA sequence, red and blue lines indicate regions of sequence homology (red to red, blue to blue), and yellow lines indicate regions with small edits. PrimeDel can introduce but does not require introduction of heterologous sequence (green). (b) Insertion of *FKBP* coding sequence fragments with PE3 (12 bp, 36 bp, 108 bp) or twinPE (108 bp) at *HEK3* in HEK293T cells. (c) Recoding of sequence within exons 4 and 7 in *PAH* in HEK293T cells using twinPE. A 64-bp target sequence in exon 4 was edited using 24, 36, or 59 bp of overlapping flaps, a 46-bp target sequence in exon 7 was edited using 22 or 42 bp of overlapping flaps, or a 64-bp sequence in exon 7 was edited using 24 or 47 bp of overlapping flaps. Editing activity was compared using standard pegRNAs or epegRNAs containing 3' evoPreQ1 motifs. (d) Schematic diagram showing three distinct dual-flap deletion strategies that were investigated for carrying out targeted deletions. The “Single-anchor (SA)” twinPE strategy allows for flexible deletion starting at an arbitrary position 3' of one nick site and ending at the other nick site. The “Hybrid-anchor (HA)” twinPE strategy allows for flexible deletion of sequence at arbitrarily chosen positions between the two nick sites. The “PrimeDel (PD)” strategy of Shendure

and co-workers tested here allows for deletion of the sequence starting at one nick site and ending at another nick site. Shaded gray boxes indicate regions where DNA is excised, red and blue lines indicate regions of sequence homology (red to red, blue to blue). **(e)** Deletion of sequences at *HEK3* in HEK293T cells using the SA-twinPE, HA-twinPE, or PD strategies targeting the same protospacer pair. Editing activity was compared using standard pegRNAs or epegRNAs containing 3' evoPreQ1 motifs. **(f)** Deletion of exon 51 sequence at the *DMD* locus in HEK293T cells using SA-twinPE, PD, paired Cas9 nuclease, or twinPE-mediated *attB* sequence replacement. A unique molecular identifier (UMI) protocol was applied to remove PCR bias (see Supplementary Note 1). Values and error bars in (b-f) reflect the mean and s.d. of three independent biological replicates.

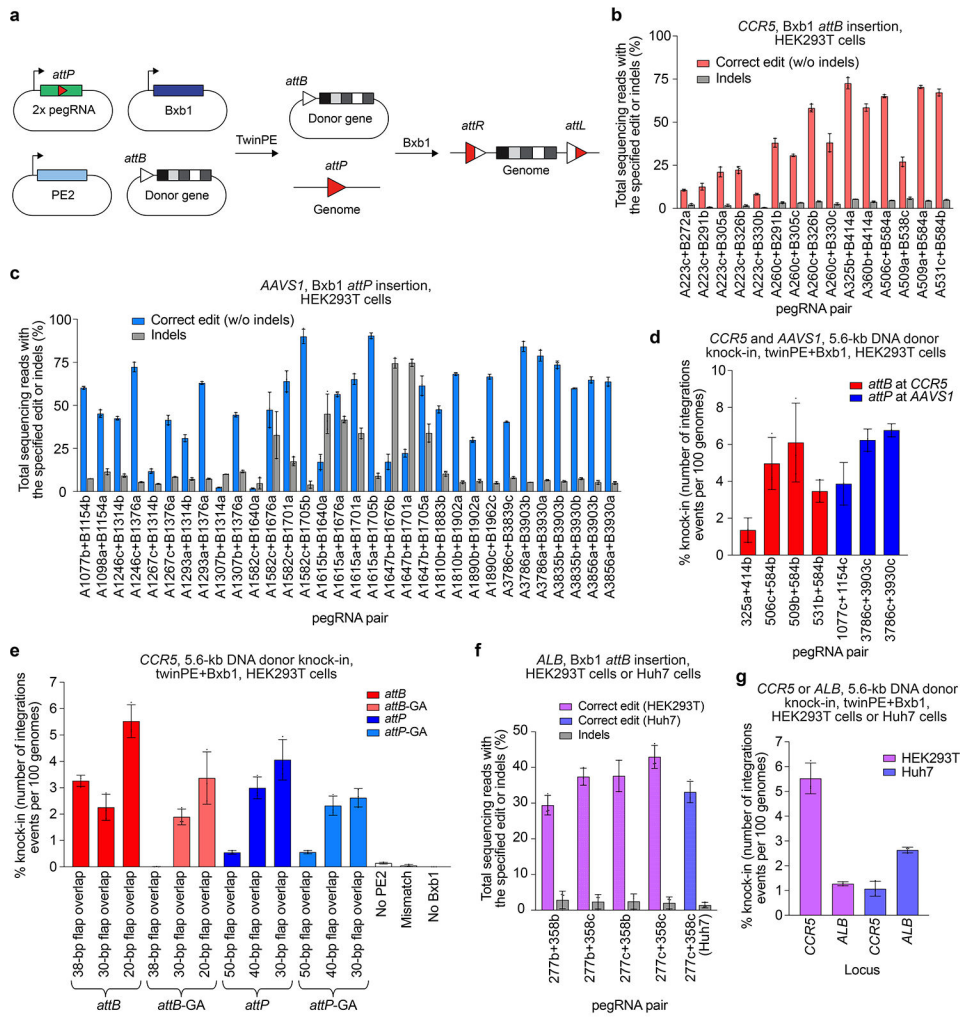


Figure 3 | Site-specific genomic integration of DNA cargo with twinPE and Bxb1 recombinase in human cells.

(a) Schematic diagram of twinPE and Bxb1 recombinase-mediated site-specific genomic integration of DNA cargo. (b) Screening of twinPE pegRNA pairs for insertion of the Bxb1 *attB* sequence at the *CCR5* locus in HEK293T cells. (c) Screening of twinPE pegRNA pairs for installation of the Bxb1 *attP* sequence at the *AAVS1* locus in HEK293T cells. (d) Single transfection knock-in of 5.6-kb DNA donors using twinPE pegRNA pairs targeting *CCR5* (red) or *AAVS1* (blue). The twinPE pegRNAs install *attB* at *CCR5* or *attP* at *AAVS1*. Bxb1 integrates a donor bearing the corresponding attachment site into the genomic attachment site. The number of integration events per 100 genomes is defined as the ratio of the target amplicon spanning the donor-genome junction to a reference amplicon in *ACTB*, as determined by ddPCR. (e) Optimization of single-transfection integration at *CCR5* using the A531+B584 spacers for the twinPE pegRNA pair. Identity of the templated edit (*attB* or *attP*), identity of the central dinucleotide (wild-type GT or orthogonal mutant GA), and length of the overlap between flaps were varied to identify combinations that supported the highest integration efficiency. % knock-in quantified as in (d). (f) Pairs of pegRNAs were assessed for their ability to insert Bxb1 *attB* into the first intron of *ALB*. Protospacer

sequences (277 and 358) are constant across the pegRNA pairs. The pegRNAs vary in their PBS lengths (variant b or c). The 277c/358c pair that performs best in HEK293T cells can also introduce the desired edit in Huh7 cells. (g) Comparison of single transfection knock-in efficiencies at *CCR5* and *ALB* in HEK293T and Huh7 cell lines. % knock-in quantified as in (d). Values and error bars reflect the mean and s.d. of three independent biological replicates.

Author Manuscript

Author Manuscript

Author Manuscript

Author Manuscript

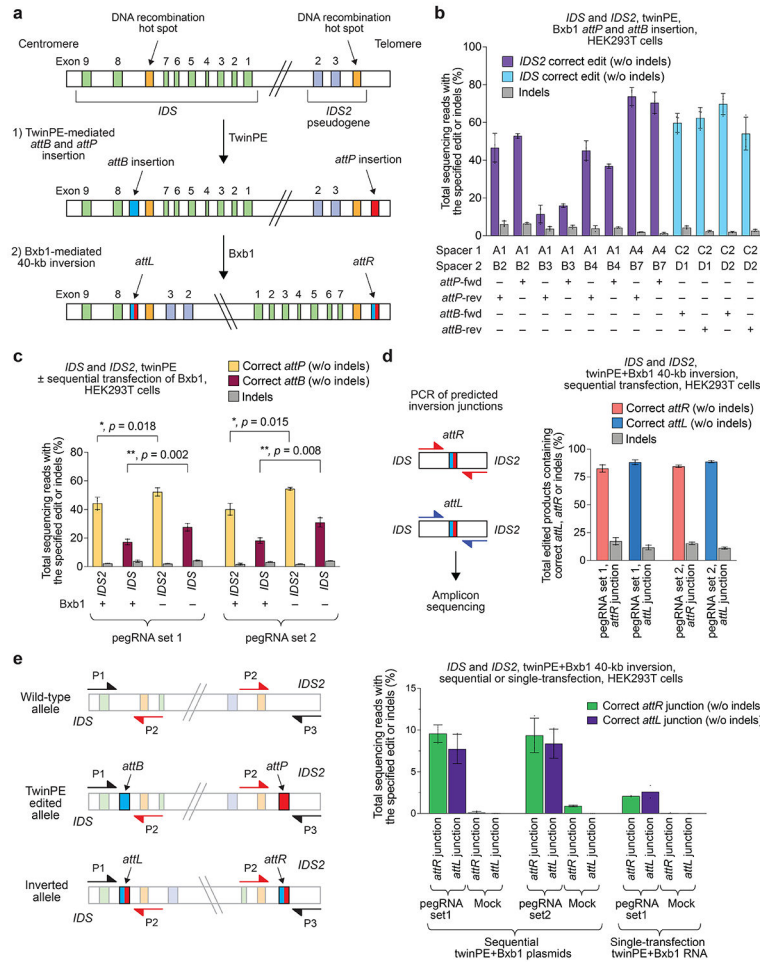


Figure 4 | Site-specific large genomic sequence inversion with twinPE and Bxb1 recombinase in human cells. (a) Schematic diagram of DNA recombination hot spots in *IDS* and *IDS2* that lead to pathogenic 39-kb inversions, and the combined twinPE-Bxb1 strategy for installing or correcting the *IDS* inversion. (b) Screen of pegRNA pairs at *IDS* and *IDS2* for insertion of *attP* or *attB* recombination sites. Values and error bars reflect the mean and s.d. three independent biological replicates. (c) DNA sequencing analysis of the *IDS* and *IDS2* loci after twinPE-mediated insertion of *attP* or *attB* sequences, with or without subsequent transfection with Bxb1 recombinase. P-values were derived from a Student’s two-tailed *t*-test. Values and error bars reflect the mean and s.d. three independent biological replicates. (d) 40,167-bp *IDS* inversion product purities at the anticipated inversion junctions after twinPE-mediated attachment site installation and sequential transfection with Bxb1 recombinase. Values and error bars reflect the mean and s.d. three independent biological replicates. (e) Analysis of inversion efficiency by amplicon sequencing at *IDS* and *IDS2* loci after sequential transfection or single-step transfection of twinPE editing components and Bxb1 recombinase. Values and error bars for sequential transfection reflect the mean and s.d. of three independent biological replicates; values for single-transfection reflect the mean of two independent biological replicates.